

# Accepted Manuscript

Diagenetic characteristics, evolution, controlling factors of diagenetic system and their impacts on reservoir quality in tight deltaic sandstones: Typical example from the Xujiache Formation in Western Sichuan Foreland Basin, SW China

Long Luo, Wanbin Meng, Jon Gluyas, Xianfeng Tan, Xianzhi Gao, Mingshi Feng, Xiangye Kong, Hengbo Shao

PII: S0264-8172(19)30074-1

DOI: <https://doi.org/10.1016/j.marpetgeo.2019.02.012>

Reference: JMPG 3725

To appear in: *Marine and Petroleum Geology*

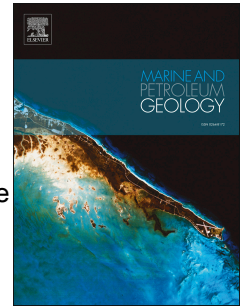
Received Date: 20 August 2018

Revised Date: 29 December 2018

Accepted Date: 11 February 2019

Please cite this article as: Luo, L., Meng, W., Gluyas, J., Tan, X., Gao, X., Feng, M., Kong, X., Shao, H., Diagenetic characteristics, evolution, controlling factors of diagenetic system and their impacts on reservoir quality in tight deltaic sandstones: Typical example from the Xujiache Formation in Western Sichuan Foreland Basin, SW China, *Marine and Petroleum Geology* (2019), doi: <https://doi.org/10.1016/j.marpetgeo.2019.02.012>.

This is a PDF file of an unedited manuscript that has been accepted for publication. As a service to our customers we are providing this early version of the manuscript. The manuscript will undergo copyediting, typesetting, and review of the resulting proof before it is published in its final form. Please note that during the production process errors may be discovered which could affect the content, and all legal disclaimers that apply to the journal pertain.



1           **Diagenetic characteristics, evolution, controlling factors of**  
2           **diagenetic system and their impacts on reservoir quality in tight**  
3           **deltaic sandstones: Typical example from the Xujiache Formation in**  
4           **Western Sichuan Foreland Basin, SW China**

5 Long Luo<sup>a,b,c,\*</sup>, Wanbin Meng<sup>d,\*\*</sup>, Jon Gluyas<sup>c</sup>, Xianfeng Tan<sup>e</sup>, Xianzhi Gao<sup>a,b</sup>, Mingshi Feng<sup>d</sup>, Xiangye Kong<sup>f</sup>,  
6 Hengbo Shao<sup>a,b</sup>

7           <sup>a</sup> State Key Laboratory of Petroleum Resources and Prospecting, China University of Petroleum, Beijing,  
8 Beijing102249, China

9           <sup>b</sup> College of Geosciences, China University of Petroleum, Beijing 102249, China

10           <sup>c</sup> Department of Earth Sciences, Durham University, Durham, DH1 3LE, UK

11           <sup>d</sup> State Key Laboratory of Oil-Gas Reservoir Geology& Exploitation, Chengdu University of Technology, Chengdu  
12 610059, China

13           <sup>e</sup> College of petroleum and gas Engineering, Chongqing University of Science and Technology,  
14 Chongqing 401331, China

15           <sup>f</sup> Unconventional Natural Gas Institute, China University of Petroleum, Beijing, 102249, China; State Key  
16 Laboratory of Petroleum Resources and Prospecting (China University of Petroleum, Beijing), Beijing 102249,  
17 China.

18 \*Corresponding author: College of Geosciences, China University of Petroleum (Beijing), Beijing 102249, China.

19 \*\*Corresponding author:

20 State Key Laboratory of Oil-Gas Reservoir Geology& Exploitation, Chengdu University of Technology, Chengdu  
21 610059, China

22 E-mail address: [longluo988@163.com](mailto:longluo988@163.com) (L. Luo). [mwb@cdut.edu.cn](mailto:mwb@cdut.edu.cn) (W. Meng).

23           **Abstract**

24           Deeply buried (3000-5000 m), deltaic sandstones of the Upper Triassic Xujiache  
25 Formation are important tight gas reservoirs in the Sichuan Foreland Basin, China.  
26 The diagenesis of these tight sandstones was examined using a variety of petrographic  
27 and geochemical techniques, including thin section description, X-ray diffraction  
28 (XRD), whole-rock chemical analysis, scanning electron microscopy (SEM),  
29 Cathodoluminescence (CL) imaging, electron probe analysis, fluid inclusions and

1 isotopic analysis. These integrated petrographic and geochemical techniques were  
2 used to determine the diagenetic history of the sandstones and its impact on the  
3 reservoir quality.

4 The tight deltaic sandstones of the  $T_3x^2$  and  $T_3x^4$  (second and fourth members of  
5 Xujiahe Formation) have undergone a significant and complicated series of diagenetic  
6 alterations and changes in geochemical composition. Strong mechanical and  
7 chemical compaction together with carbonate cementation destroyed almost all the  
8 primary pores and the secondary dissolution pores now dominate the pore space. The  
9  $T_3x^4$  sandstones experienced a more open diagenetic system at near-surface and  
10 eodiagenesis resulted in higher porosity than seen in the  $T_3x^2$  sandstones. Both the  $T_3x^2$   
11 and  $T_3x^4$  sandstones experienced closed-system diagenesis during middle-late  
12 mesodiagenesis. The early diagenetic dissolution, which mainly occurred in the open  
13 geochemical system, produced secondary pores and provided kaolinite and some  $K^+$   
14 needed for the subsequent illitization of kaolinite and K-feldspar. The late dissolution  
15 of K-feldspar and illitization of K-feldspar in  $T_3x^4$  sandstones and  $T_3x^2$  sandstones  
16 during the mesodiagenesis, produced some effective secondary pores in the closed  
17 geochemical system or in the focused fluid flow zone along fractures. The diagenetic  
18 characteristics, size and evolution of (open vs closed) diagenetic system, which were  
19 constrained by the depositional environment, deep burial depth and tectonic activity,  
20 can be used to predict the reservoir quality ahead of drilling.

21 **Keywords:**

22 Tight deltaic sandstone; Diagenetic system; Mass transfer; Deep burial; Reservoir  
23 quality; Xujiahe Formation; Western Sichuan Foreland basin

24 **1. Introduction**

25 The concept of a diagenetic system was first proposed in the 1970s and 1980s,

1 when sandstone diagenesis and the diagenetic alteration of adjacent mudstones were  
2 discussed together as systems (Boles and Franks, 1979; Surdam et al., 1989; Gluyas  
3 and Coleman,1992). Only a few articles discuss diagenesis in terms of open and  
4 closed system in terms of element mobility during the processes of mineral  
5 precipitation and dissolution (Gluyas and Coleman, 1992; Gluyas et al, 2000;  
6 Day-Stirrat et al., 2010; Bjørlykke, 2011; Day-Stirrat et al., 2011; Bjørlykke and  
7 Jahren, 2012; Yuan et al., 2015a; Yuan et al., 2015b; Yuan et al., 2017a; Yuan et al.,  
8 2017b). For a closed diagenetic system, the bulk chemical composition of the  
9 sediment does not change significantly during burial diagenesis, and there is a mass  
10 balance between mineral dissolution and precipitation (Bjørlykke and Jahren, 2012).  
11 On the contrary, the open diagenesis system is characterized by the significant  
12 enrichment or reduction in bulk chemical composition for some elements owing to the  
13 fluid flow and transport of solutes into or out of the system (Bjørlykke and Jahren,  
14 2012; Bjørlykke, 2014; Yuan et al.,2015b). There is evidence of open system  
15 diagenesis (Gluyas and Leonard,1995; Day-Stirrat et al., 2010; Day-Stirrat et al., 2011;  
16 Bjørlykke and Jahren, 2012; Yuan et al., 2015b) and of closed system diagenesis  
17 especially during deep burial because of limited flow rate and concentration gradients  
18 of pore-water flow (Gluyas et al, 2000; Clark, 2014).

19 In a closed diagenetic (geochemical) system, predictions about rock properties or  
20 reservoir quality can be achieved with respect to rock properties as a function of  
21 burial history and diagenetic reactions and sediment composition (Gluyas, 1997;  
22 Gluyas and Witton, 1997) and written as balanced chemical equations (Bjørlykke,  
23 2010; Bjørlykke and Jahren, 2012). However, the reservoir quality is not easy to  
24 forecast in the open diagenesis system, because the diagenetic characteristics (type,  
25 sequence and origin) and controlling factors are complex and changeable and the

1 processes of mass and transport required for an open system are rarely well  
2 understood (Bjørlykke and Jahren, 2012; Bjørlykke .2014).

3 The deltaic sandstone of the Upper Triassic Xujiahe Formation is an important  
4 tight gas reservoir in the Western Sichuan Foreland Basin of China (Tang et al., 2009).  
5 The deeply buried, tight deltaic sandstone of the Upper Triassic Xujiahe Formation  
6 have generally undergone complicated diagenetic alterations which have reduced the  
7 reservoir quality (Meng et al.,2013; Liu et al.,2014a, b; Luo et al.,2015). The Xujiahe  
8 Formation may have experienced an open diagenetic system during burial process  
9 because it experienced several hydrogeological and tectonic (fracture formation)  
10 events within its geological history (Zheng et al., 2003; Shen et al., 2010).

11 The aim of this study was to understand the diagenetic evolution of tight gas  
12 sandstones belonging to the Triassic, Xujiahe Formation, Sichuan Foreland Basin, SW  
13 China (Fig.1) in order that in unexplored regions of the basin the reservoir quality can  
14 be forecast ahead of drilling. Both porosity and permeability are generally low in the  
15 Xujiahe Formation but there are intervals with higher permeability ( $>0.1\text{mD}$ ) that  
16 dominate gas flow and as such it is necessary to understand how the diagenetic system  
17 evolved in order to forecast the occurrence of such zones.

## 18 **2. Geological setting**

### 19 **2.1 Basin evolution**

20 The Sichuan Basin, in southwestern China, is a diamond-shaped foreland basin  
21 surrounded by thrust belts on all sides (Xu et al., 2015) (Fig. 1). This superimposed  
22 basin has undergone two tectonic and corresponding depositional cycles: the  
23 Sinian-Middle Triassic tectonic evolution of a passive continental margin and the Late  
24 Triassic-Eocene evolution of a foreland basin (Ni et al., 2014, Lai et al., 2015). From  
25 the Early to Middle Triassic, the cratonic margins of the Sichuan Basin were raised as

1 a result of the compression of the Tethys and Pacific Plates (Lai et al., 2015). In the  
2 Late Triassic, the Sichuan Basin evolved into a foreland basin with the uplift of the  
3 Longmen Mountain at its western margin (Tao et al., 2014); therefore, the Western  
4 Sichuan foreland basin, located in the Western Sichuan Basin, developed after the  
5 Late Triassic (Fig. 1, Wang, 2012).

6 The Xinchang structural belt, located in the central region of the Western  
7 Sichuan Foreland Basin (depression, Fig. 1), is a large multistage uplift that began in  
8 the late Indo-Chinese epoch (Late Triassic), developed during the Yanshanian Period  
9 (Triassic - Cretaceous), and eventually finished forming during the Himalayan (Ye et  
10 al., 2009).

## 11 **2.2. Stratigraphy and depositional facies**

12 The stratigraphic column of the Western Sichuan depression shows that the  
13 Upper Triassic Xujiahe Formation (roughly equivalent to the Upper Triassic Norian  
14 stage) generally comprises its second member ( $T_3x^2$ ), third member ( $T_3x^3$ ), fourth  
15 member ( $T_3x^4$ ) and fifth member ( $T_3x^5$ ) (Fig. 2) (Zheng et al., 2003). The first member  
16 of the Xujiahe Formation ( $T_3x^1$ ), which represents the critical source rock, is generally  
17 divided into the Xiaotangzi and Maantang intervals, because it was deposited in  
18 shallow sea or marine prodelta environment that was significantly different from the  
19 continental or transitional environments of other members of the Xujiahe Formation,  
20 (Lin, 2005). The second ( $T_3x^2$ ) (burial depth >4600m; thickness 560-660m) and fourth  
21 ( $T_3x^4$ ) (burial depth 3000-4000m; thickness 536-610m) members of the Xujiahe  
22 Formation mainly consist of deltaic sandstones, which are the major sandstone  
23 reservoirs of the study area (Fig. 2). The second member of the Xujiahe Formation  
24 ( $T_3x^2$ ) was mainly deposited in a marine delta front belonging to a  
25 marine-to-continent transitional environment, which mainly consists of

1 distributary channel and mouth bar sandstones (Lin, 2005; Shi,2010). However,  
2 the fourth member ( $T_3x^4$ ) was deposited in the lacustrine braided-river delta front  
3 of continent sedimentary environment, in which, underwater distributary channel  
4 and mouth bar are the dominant microfacies (Lin, 2005; Shi,2010). The third ( $T_3x^3$ )  
5 and fifth( $T_3x^5$ ) members of the Xujiahe Formation were deposited in a lacustrine  
6 braid-river delta plain that is dominated by swamp microfacies and branch  
7 channel, so both the  $T_3x^3$  and  $T_3x^5$  are important source rocks and coal-bearing  
8 strata (Lin, 2005; Shi, 2010).

### 9 **2.3 Diagenetic geochemical system**

10 Fractures are important fluid-flow conduits and a significant part of the reservoir  
11 pore volume in the Xujiahe Formation (Zhang, 2005; Zeng, 2010; Luo, 2015). The  
12 fractures were controlled by the tectonic activity and are critical to large-scale  
13 convection of fluid in the reservoir because of their high permeability (Zhang, 2005;  
14 Zeng, 2010). The fractures in the  $T_3x^2$  member started to form at the end of the  
15 Triassic (the Late Indosinian), and continued forming during the Yanshanian and  
16 Himalayan (Zhang, 2005). The initial stage of fracturing within the  $T_3x^4$  member was  
17 at the end of the Middle Yanshanian, and subsequent stages were late Yanshanian and  
18 Himalayan (Zhang, 2005). Consequently, the abundant fractures in the Xujiahe  
19 Formation provide crucial migration pathways for fluid flow and transport of solutes .

20 Cross-formational migration of fluids in the Upper Triassic drove  
21 homogenisation of formation water geochemistry in the  $T_3x^2$  and  $T_3x^4$  members  
22 (Zheng et al., 2003; Shen et al 2010). The original formation water within the  $T_3x^2$   
23 and  $T_3x^4$  were almost completely replaced by the formation water from the  
24 coal-bearing strata (e.g.  $T_3x^3$  and  $T_3x^5$ ) and the underlying marine mudstone of the  
25  $T_3x^1$  member (Shen et al., 2010). These previous studies indicate the possible

1 existence of an open geochemical system in the Xujiahe Formation ( $T_3x^2$  and  $T_3x^4$ )  
2 during burial process from near-surface to deep burial (Liu, 2010; Shen et al., 2010).

### 3 **3. Materials and methods**

4 Rock composition data for 7068 thin sections samples (4254 from  $T_3x^2$  and 2814  
5 from  $T_3x^4$  of related 32 wells) and 6550 porosity and permeability data pairs (2760  
6 from  $T_3x^2$  core sandstone samples and 3790 from  $T_3x^4$  sandstone) were provided by  
7 the Research Institute of Petroleum Exploration & Development of the Southwest  
8 Oil-Gas Branch Company, Sinopec.

9 Based on the objectives of this study, 250 sandstone samples (sampling interval  
10  $\sim 0.5$  m) were collected from the  $T_3x^2$  and  $T_3x^4$  members in drill cores of 32 wells (Fig.  
11 1C), in which 220 thin sections (18 key wells with hydrocarbon shows) were  
12 impregnated with blue epoxy resin and prepared for mineralogical and diagenetic  
13 studies (Fig. 1C). Thin sections were partly stained with Alizarin Red S and  
14 K-ferricyanide for carbonate mineral identification. Point counting (300 points per  
15 thin section) analysis, in which the composition of 300 points per thin-section will  
16 be identified and counted, was performed on 40 thin sections collected from 40 drill  
17 cores of  $T_3x^2$  and  $T_3x^4$  members in 10 key wells to quantify rock composition and  
18 confirm the previously collected rock composition data and diagenetic relationships  
19 (Van der Plas and Tobi, 1965; Yuan et al., 2015a,b; Hansen et al., 2017). Cements in the  
20 40 thin sections were identified and photographed under the microscope with digital  
21 camera and sketched on a computer using the CorelDRAW software, and the  
22 corresponding area of each cement in the photomicrographs was calculated using  
23 Image-Pro Plus software. Finally, the bulk percentage of each cement was calculated  
24 by determining the average value of area rates in 10 photomicrographs from the same  
25 thin section.



1 150 core representative samples (from the main reservoir sandstone of key wells  
2 with hydrocarbon shows) were coated with gold and examined under a Quanta250  
3 FEG scanning electron microscope (SEM) equipped with an Oxford INCAx-max20  
4 energy dispersive spectroscope (EDS). Cathodoluminescence (CL) analyses of 20  
5 typical core samples, in which carbonate cement was relatively well developed  
6 (> 2%), were completed using an Olympus microscope equipped with a  
7 CL8200-MKS CL instrument.

8 Eighty-five carbonate grains, including carbonate cements and rock fragments,  
9 were analysed for their C and O isotopic compositions in situ using the laser  
10 microsampling technique with a MAT252 Gas Isotope Ratio Mass Spectrometer at the  
11 Research Institute of Exploration and Development of the Southwest Oil-Gas field  
12 Company, Petrochina. The selected carbonate minerals produced CO<sub>2</sub> gas by heating  
13 the specified micro-zone of thin-section inside the vacuum sample box with  
14 high-energy laser beam. Then the CO<sub>2</sub> gas was purified by vacuum and sent into mass  
15 spectrometer for measurement of carbon and oxygen isotope. The precision was  $\pm 0.08\%$   
16 for oxygen and  $\pm 0.06\%$  for carbon.

17 Twenty core samples with quartz cement (more than 2%) were prepared as thick  
18 doubly polished sections of 100  $\mu\text{m}$  thickness for microthermometric measurement of  
19 fluid inclusions using a petrographic microscope equipped with a Linkam. The  
20 THMSG 600 heating and cooling stage enables the temperatures of phase transitions  
21 ranging from -180 to 600°C. Inclusions within quartz cement were photographed with  
22 digital camera for the purpose of fast mapping of inclusion locations. The  
23 homogenization temperature (Th) were determined for inclusions inside quartz  
24 cement using a heating rate of 10°C/min (18°F/min) when the temperature was lower  
25 than 70°C (158°F) and a rate of 5°C/min (9°F/min) when the temperature exceeded

1 70°C (158°F). The measured temperature precision for Th is  $\pm 1^\circ\text{C}$  ( $\pm 1.8^\circ\text{F}$ ).

2 X-ray diffraction (XRD) analysis of whole-rock samples and quantitative clay  
3 minerals were performed on 65 core samples (32 samples from  $T_3x^2$  and 33 samples  
4 from  $T_3x^4$ ) to identify species and contents of major minerals, relative contents of  
5 different clay minerals and I/S mixed-layer ratios. The whole-rock chemical analysis  
6 was performed on 65 sandstone samples for the content of major elements using  
7 direct-reading spectroscopy method of full spectrum (ICP-AES) under condition of 20□  
8 temperature and 65% humidity. The rock samples were ground to fine powder and  
9 homogenized. Approximately 0.25 g of the powder was dissolved in a mixture of hot  
10 hydrofluoric and hydrochloric acids. The resultant solutions were diluted with  
11 distilled water before analysis. The solutions were analysed, using inductively coupled  
12 plasma atomic emission spectrometry (ICP), for aluminium, titanium, iron,  
13 manganese, calcium, magnesium, potassium and sodium (Gluyas and Coleman, 1992).  
14 Silicon was obtained by gravimetric methods. Precision on whole-rock analysis is  
15 estimated to be within +1% (Gluyas and Coleman, 1992).

16

## 17 **4. Results**

### 18 **4.1 Sandstone petrography**

19 The  $T_3x^2$  sandstones mainly comprise litharenite and minor feldspathic  
20 litharenite, and the  $T_3x^4$  sandstones consist of major litharenite and minor lithic quartz  
21 arenite (Fig. 3A-B, Table 1). The sandstone classification was based on the standard of  
22 Folk et al., 1970 (Fig. 3A-B). The feldspars within the  $T_3x^2$  and the  $T_3x^4$  consist of  
23 plagioclase (major albite and minor calcic plagioclase) and K-feldspar (Table 1, Table  
24 2). The rock fragments of the  $T_3x^2$  and  $T_3x^4$  sandstone mainly comprise fragments of  
25 major sedimentary rocks (e.g. limestone, dolomite and mudstone), fragments of

1 metamorphic rock (e.g. phyllite, slate and shist) and small amounts of volcanic rocks  
2 (e.g. basalt and andesite). The  $T_3x^4$  sandstones have more sedimentary and volcanic  
3 rock fragments and less detrital quartz than the  $T_3x^2$  sandstones (Table 1). Carbonate  
4 rock including micrite limestone and dolomite is dominant in the sedimentary rock  
5 fragments of  $T_3x^2$  and  $T_3x^4$  sandstones. The  $T_3x^2$  sandstones and  $T_3x^4$  sandstones  
6 mainly comprise major medium-grained, minor fine-grained and 6.3% coarse-grained  
7 sandstones.

## 8 **4.2 Diagenetic minerals and alterations**

### 9 **4.2.1 Compaction**

10 Framework grains in the Xujiahe Formation sandstones ( $T_3x^2$  and  $T_3x^4$ ) are  
11 generally heavily compacted (both mechanically and chemically), as is indicated by  
12 the dominance of long and concave-convex grain contacts (Fig. 4A-F). Direct  
13 evidence of mechanical compaction, which has mostly occurred in the  $T_3x^4$ , are the  
14 deformation of mica and plastic rock fragments (Fig. 4A, B, E, F). Chemical  
15 compaction, pressure dissolution, observed in  $T_3x^2$ , is manifested by the concave-  
16 convex and sutured contacts between quartz grains (Fig. 8A-B, Fig. 4C, D). However,  
17 compaction is obviously less extensive in sandstones with chlorite rims than in other  
18 rocks within the  $T_3x^2$  (Fig. 11G-I).

### 19 **4.2.2 Carbonate cements**

20 Carbonate cements are the dominant cement in the sandstones. They occur as  
21 scattered euhedral rhomb and pore-filling blocky and mosaic aggregates in the  $T_3x^2$   
22 and  $T_3x^4$  tight sandstones (Fig. 5, Fig. 6). In the  $T_3x^2$  tight sandstones, carbonate  
23 cements with an average of 6.68% mainly consist of calcite (av.vol 3.72%) and  
24 dolomite (av. vol 2.96%) (Table 1). The calcite generally occurs as isolated blocky  
25 sparite cements filling intergranular pores (pore diameter,  $50\mu\text{m}\sim 120\mu\text{m}$ , (Fig. 5A)

1 and as partial replacements of detrital grains (e.g. feldspars and volcanic rock  
2 fragments, Fig. 5D, E). Dolomite also occurs as pore-filling poikilotopic sparite  
3 patches that fill intergranular pores (pore diameter,  $50\ \mu\text{m}\sim 200\ \mu\text{m}$ , Fig. 5B) or as  
4 euhedral rhomb (single crystal:  $40\ \mu\text{m}\sim 120\ \mu\text{m}$ ) and partial replacements of detrital  
5 grains (e.g. feldspar) filling intragranular pores (Fig. 5D- F).

6 The carbonate cement has an average content of 5.92% in the  $T_3X^4$  sandstones, of  
7 which 4.97% is calcite and 0.95% is dolomite (Table 1). Calcite cements mostly occur  
8 as microcrystalline sparite (single crystal:  $10\ \mu\text{m}\sim 50\ \mu\text{m}$ ), poikilotopic masses that  
9 fills in primary (intergranular) pores (Fig. 6A-C), and as partial replacements of  
10 detrital grains (e.g. feldspars and rock fragments) that fill secondary pores  
11 (intergranular and intragranular dissolved pores) and accompany partial dissolution  
12 and kaolinization of feldspar (Fig. 6D-F). The minor (0.95%) sparite dolomite (single  
13 crystal:  $30\ \mu\text{m}\sim 80\ \mu\text{m}$ ) generally occur as partial replacements of detrital grains (e.g.  
14 carbonate rock fragments), and accompany the dissolution of carbonate rock  
15 fragments (Fig. 6D).

16 The primary and secondary intergranular pores, filled with calcite/dolomite  
17 cements, can be distinguished by thin-section analysis that were impregnated with  
18 blue epoxy resin or the scanning electron microscope analysis (SEM). The primary  
19 pores that are filled with calcite cement generally have regular edges which abut  
20 against the original detrital grains (Fig. 5A, Fig. 6A-B). However, the secondary  
21 intergranular pore is characterized by irregular edges that are formed by partial  
22 dissolution and replacement of calcite around the detrital grains (feldspar)(Fig. 6A-B).  
23 Feldspars that are partly replaced by calcite are generally accompanied by dissolution  
24 in the  $T_3X^2$  and  $T_3X^4$  sandstones (Fig. 5D-F-, Fig. 6D-F). CL micrographs show that  
25 the carbonate cements of the Xujiahe Formation sandstones can be divided into two

1 generations of early and late carbonate cement (Fig. 6B). The saffron yellow  
2 micro-crystal calcite that fills primary pores, which represent the first  
3 generation, precipitated before strong mechanical compaction as evidenced by the  
4 floating detrital grains and point contacts between grains (Fig. 6B). The orange red  
5 calcite that mostly fills the residual primary pore and secondary pores and partially  
6 replaced some detrital grains, represents the second generation (Fig. 6 B). The calcite  
7 cements of  $T_3X^4$  sandstone consist of major early calcite and minor late calcite, but the  
8  $T_3X^2$  sandstone was dominated by late calcite.

9 Electron microprobe (EMP) analyses reveal the molar compositional fraction of  
10 carbonate cements in the  $T_3X^2$  sandstone and the  $T_3X^4$  sandstone (Table 4). The  
11 calcite cements have nearly similar molar compositional fraction between the  $T_3X^2$   
12 sandstone and the  $T_3X^4$  sandstone (Table 4). Besides, almost all of dolomite cements  
13 occur in the  $T_3X^2$  sandstones and rarely in the  $T_3X^4$  sandstones (Table 4). The dolomite  
14 should be classified as the ankerite for abundant  $FeCO_3$  (av. 20.86%, Table 4).

15 The  $\delta^{18}O_{V-PDB}$  and  $\delta^{13}C_{V-PDB}$  values of calcite cements in the primary pores are  
16 similar to that of the calcite rock fragments and that of carbonate rock fragments in  
17 the  $T_3X^4$  sandstones (Fig. 7A, Table 5). The dolomite (ankerite) crystals filling in the  
18 secondary pores have lower  $\delta^{18}O_{V-PDB}$  values and similar  $\delta^{13}C_{V-PDB}$  values in  
19 comparison to that of the calcite in primary pores in the  $T_3X^4$  sandstones (Fig. 7A,  
20 Table 5). The  $\delta^{18}O_{V-PDB}$  and  $\delta^{13}C_{V-PDB}$  values of calcite cements in the secondary pores  
21 are obviously more negative than that of other carbonate in the  $T_3X^4$  sandstones (Fig.  
22 7A, Table 5).

23 In the  $T_3X^2$  sandstones, the  $\delta^{18}O_{V-PDB}$  values and  $\delta^{13}C_{V-PDB}$  values of calcite  
24 cements are similar to that of dolomite (ankerite) cements ((Table 6, Fig. 7B). The  
25 dolomite fragments have similar  $\delta^{18}O_{V-PDB}$  values and slightly higher  $\delta^{13}C_{V-PDB}$  values

1 (Table 6, Fig. 7B).

### 2 **4.2.3 Quartz cements**

3 Point counting of thin section, cathodoluminescence, and SEM analyses indicate  
4 that authigenic quartz is the second most abundant cement after carbonate. Quartz  
5 cements generally occur as syntaxial overgrowths (thickness 20 $\mu$ m to 120 $\mu$ m) that  
6 partially coat of detrital quartz grains (Fig. 8A-C, Fig. 8F) or as isolated pore-filling  
7 quartz crystal (Fig. 8D, E, Fig. 8G). Quartz overgrowths are usually accompanied  
8 by sutured (microstylolitic) quartz grains contacts (Fig. 8A, F, I). The isolated  
9 pore-filling authigenic quartz crystal are generally accompanied by the dissolution of  
10 feldspar and some illite (Fig. 8E, H), indicating that the isolated pore-filling quartz  
11 crystals are like to be related to the dissolution of feldspar (Hawkins, 1978; Worden  
12 and Morad,2000).

13 The quartz cement of the T<sub>3</sub>x<sup>2</sup> sandstones has an average content of 2.16%,  
14 which represents 24.4% of the total cement content (Table 1). Moreover, the quartz  
15 cement content increases with increasing amounts of detrital quartz in the T<sub>3</sub>x<sup>2</sup>  
16 sandstones (Fig. 9). In the T<sub>3</sub>x<sup>4</sup> sandstones, quartz cement generally occurs as isolated  
17 pore-filling quartz crystals or syntaxial overgrowths (Fig. 8B, Fig. 8E-G); this quartz  
18 cement has an obviously low average content of 0.94%, which represents 13.2% of  
19 the total cement content (Table 1).

20 The homogenization temperatures of fluid inclusions in quartz cements reveal  
21 that crystallization temperature of quartz cements in the T<sub>3</sub>x<sup>2</sup> sandstones ranges from  
22 50 to 90°C, 100 to 140°C and 150 to 190°C and that those of the T<sub>3</sub>x<sup>4</sup> sandstones  
23 mostly range from 90 to 150 °C (Fig. 10). In addition, the homogenization  
24 temperatures of aqueous inclusions in authigenic quartz within fractures range from  
25 50 to 60°C and 170 to 330°C.

#### 1 4.2.4 Clay minerals

2 Illite, chlorite, kaolinite and minor mixed-layer illite/smectite (less than 1% of  
3 the clay minerals), were revealed by XRD and SEM analyses (Table 2, Table 3).  
4 Illite, which represents 46.8% (average) of clay mineral in  $T_3x^2$  and 43% (average) in  
5  $T_3x^4$  sandstones, occurs mainly as grain-coatings, nested aggregates filling in  
6 secondary intragranular dissolved pores and non-netted aggregates filling in  
7 intergranular spaces (Fig. 11A-F, Meng et al., 2011). The nested illites are generally  
8 accompanied by the dissolution of feldspar and rock fragments (Fig. 11A, B, E, F);  
9 non-netted aggregates may be related to the illitization of the matrix consisting of  
10 smectite (Fig. 11C, O). The  $T_3x^2$  sandstones have a higher chlorite content (av. 2.4,  
11 whole rock %; av. 51.9 clay %) than the  $T_3x^4$  sandstones (av. 1.6, whole rock %; av.  
12 26.1 clay %) (Table 2, Table 3, Fig. 12, Fig. 13). Chlorite rims are partly  
13 well-developed in the  $T_3x^2$  which can be observed under cross-polarizing light and  
14 SEM analysis (Fig. 11G-I). However, in the fourth member ( $T_3x^4$ ), chlorite cement is  
15 dominated by authigenic pore-filling chlorite (Fig. 11K), and some chlorite appears  
16 as chloritized of rock fragments (Fig. 11J).

17 Kaolinite, which represents 0% to 72 % (av.28.5%) of all clay minerals, mostly  
18 occurs at the top of the  $T_3x^4$  sandstones and is nearly absent in the  $T_3x^2$  sandstones  
19 (Table 2, Table 3, Fig. 12, Fig. 13, Fig. 14B). Kaolinite generally occurs as vermicular  
20 or booklet-like aggregates of pseudo-hexagonal crystals (Fig. 11L~M). They are  
21 usually observed in secondary pores associated with feldspar dissolution (Fig. 11M).  
22 In addition, some booklet-like pseudo-hexagonal kaolinite has transformed into  
23 filamentous illite (Fig. 11N). Small amounts of flaky smectite are present in the  
24 mixed-layer illite/smectite (Table 4, Fig. 11O).

#### 25 4.2.5 Dissolution

1 Secondary pores, which are the most important pore type in the studied  
2 sandstones, were generally formed by the dissolution of major feldspars and minor  
3 volcanic rock fragments (point counting) (Fig. 15A-F). Secondary pores mostly occur  
4 at the top of  $T_3x^4$ ; others occur at the bottom of  $T_3x^4$  and in the middle-upper part of  
5  $T_3x^2$  (Fig. 16). Overall, the dissolution is more prevalent in  $T_3x^4$  than  $T_3x^2$  sandstone  
6 (Fig. 4, Fig. 16). Detrital K-feldspar grains have experienced partial to complete  
7 dissolution (Fig. 15A-C). Feldspar dissolution is generally accompanied by the  
8 formation of some authigenic kaolinite and quartz (Fig. 11-M, Fig. 15B).

### 9 **4.3 Pore types, porosity and permeability**

10 The pore space of  $T_3x^2$  sandstone consists of primary pore (av.0.84%), secondary  
11 dissolved pore (av.0.79%) and fracture (0.23%) (Fig. 17). The pore space of  $T_3x^4$   
12 sandstone comprises major secondary dissolved pore (av.3.49%), minor primary pore  
13 (av.0.58%) and fracture (0.09%) (Fig. 17).

14 The core porosity of  $T_3x^2$  sandstone mainly ranges from 1% to 5% (av.3.44%),  
15 and the core permeability ranges from 0.02 to 0.16mD (av.0.089mD). In the  $T_3x^4$   
16 sandstones, core porosity generally characterized by two main ranges of 1%–3%  
17 and 3%–9% (av.5.14%), the core permeability ranges from 0.02 to 0.32mD  
18 (av.1.08mD).

19 In porosity-depth and permeability-depth profiles, both porosity and permeability  
20 of  $T_3x^2$  and  $T_3x^4$  sandstones show wide variation at shallow to deep depths (Fig. 18).  
21 Porosity and permeability generally decrease with increasing burial depth. However,  
22 porosity and permeability values of P10 (10% of reservoirs have porosity higher than  
23 this value) and P50 (median) curves show that some higher porosity and permeability  
24 intervals exist in the  $T_3x^2$  and  $T_3x^4$  sandstones (Fig. 18).

25



#### 1 4.4 Sandstone geochemistry

2 The major elements (whole rock) of  $T_3x^2$  sandstones and  $T_3x^4$  sandstones  
3 comprise  $Na_2O$ ,  $K_2O$ ,  $MgO$ ,  $Fe_2O_3$ ,  $TiO_2$ ,  $Al_2O_3$ ,  $SiO_2$  (Table S1, Table S2). The  $MgO$ ,  
4  $K_2O$ ,  $Al_2O_3$  contents of  $T_3x^4$  sandstone have obvious vertical changes, but that of  $T_3x^2$   
5 sandstone present relatively fixed values in vertical profile (Fig. 12A, Fig. 13A).

#### 6 5. Discussion

##### 7 5.1 Mechanism and time of dissolution

8 The types of pore space and the porosity-depth and permeability-depth profiles  
9 indicate that the dissolution of minerals was the most important source of pore space  
10 creation in the  $T_3x^2$  and  $T_3x^4$  sandstones (Fig. 17, Fig. 18). For dissolution to occur the  
11 pore fluids need to be under saturated with respect to the detrital minerals. Under  
12 saturation can come about simply from increased temperature during burial or from a  
13 change in composition of the pore fluid caused ingress of new pore fluids. A  
14 candidate fluid that would promote dissolution is an acidic one and we know that  
15 organic acids would have been formed from the thermal maturation of coal in the  
16 adjacent  $T_3x^3$  and  $T_3x^5$  members.

17 Coal-bearing stratum produce many kinds of organic acids during early diagenetic  
18 stage (Kauss et al., 1997; Dias et al., 2002) and peak at temperature range of  $80^\circ C$  to  
19  $140^\circ C$  (Surdam et al., 1989; Zeng et al., 2007). The amount of organic acids generated  
20 by coal-bearing strata ( $T_3x^3$  and  $T_3x^5$ ) is generally 2-5 times higher than other kinds of  
21 source rock ( $T_3x^1$ ) (Zheng and Ying, 1997; Yuan et al., 2013). Feldspar dissolution,  
22 secondary pores and enlarged dissolution of micro-fractures are prevalent in the  
23 studied sandstones (Fig. 14, Fig. 15A-C, Fig. 15F, Fig. 16, Fig. 17). Fig. 17, Besides, the  
24 distribution of secondary pore is related to source rocks (Fig. 16A-D). These indicate  
25 that acidic fluids from source rocks migrated and flowed into the  $T_3x^2$  and  $T_3x^4$

1 sandstones through these fractures, meanwhile provoked pervasive dissolution in  
2 studied sandstones (Fig. 15F). Hence, the feldspar dissolution of the  $T_3x^4$  and  $T_3x^2$   
3 sandstones may occur from eodiagenesis to mesodiagenesis stage (60°C-140°C).

4 Secondary pores are mostly distributed on the top of  $T_3x^4$ , where they  
5 approximately correspond to the zone containing decreasing amounts of feldspars, the  
6 development of kaolinite and the skewness/rapid change of the Ro value, and more  
7 prevalent than the middle part of  $T_3x^4$  (Fig. 14, Fig. 16)..Therefore, feldspar  
8 dissolution recorded at the top of the  $T_3x^4$  might be caused by acidic fluids from the  
9 coal-bearing formation of the  $T_3x^5$  . Besides, there is an extensive II-type  
10 unconformity on the top of the  $T_3x^4$  (Zhang, 2011). As such some early dissolution  
11 might come from leaching by low-pH meteoric waters containing CO<sub>2</sub> gas phase .

12 However, there are not more secondary pores (Fig. 16A-D) and higher core  
13 porosity (Fig. 18A) at the bottom of  $T_3x^2$  than there are in the middle-upper part, even  
14 if they are adjacent to the Xiaotangzi Formation ( $T_3x^1$ ), which mainly consist of the  
15 source-rock (Fig. 2). This may be explained by the fact that obviously thinner  
16 sandstone, less feldspar, more alkaline diagenetic environment in the bottom of the  
17  $T_3x^2$  consisting of similar marine mudstone interbedded with sandstone than there is  
18 in the middle-upper part , which resulted in less feldspar dissolution in sandstones  
19 (Fig. 2). In addition, some few rock fragments (e.g. carbonate and volcanic rock  
20 fragments) were dissolved together with feldspars by these acidic fluids (Fig. 15D,  
21 E).

## 22 **5.2 Genesis of diagenetic minerals**

### 23 **5.2.1 Source, temperature and time of carbonate diagenesis**

24 Carbonate cements have many potential carbon sources including internal and  
25 external sources (Gier et al., 2008; El-Ghali et al., 2013; Luo et al.,2018). The

1  $\delta^{18}\text{O}_{\text{water}}$  values of parent diagenetic pore water of the calcites filling primary pores  
2 comprising the meteoric and marine water within the  $T_3x^4$  are approximate -3‰  
3 SMOW, and that of current pores water in the  $T_3x^4$  range from -4.3‰ to +0.5‰  
4 (SMOW) with an average value of -1.4‰ (SMOW) (Shen et al, 2010; Liu et al,  
5 2014a,b). The  $\delta^{18}\text{O}_{\text{water}}$  values of parent diagenetic pore water of carbonate cements  
6 in the  $T_3x^2$ , which was deposited in marine water, were nearly 0‰ SMOW, and the  
7  $\delta^{18}\text{O}_{\text{water}}$  values of current pore water range from -4.5‰ to -1.3‰(SMOW) (Shen et al,  
8 2010;Liu et al, 2014a,b). Using oxygen isotope fractionation factor for calcite-water  
9 from Friedman and O'Neil (1977), the precipitation temperatures for different types of  
10 carbonate cements can be calculated (Table 5, Table 6, Fig. 18, Fig. 19).

11 The early calcite cements filling the primary pores of the  $T_3x^4$  sandstone (-10.06‰  
12 to -4.75‰, av. +7.38‰) were calculated to be precipitated at approximately 30-65°C  
13 (Table 4, Fig. 19A). Moreover, nearly poikilotopic calcite cements filling in primary  
14 (intergranular) pores mostly occur as microcrystalline to sparite (Fig. 6A,C), which  
15 also indicate that calcite precipitated at the early diagenetic stage. The calcites filling  
16 the primary pores of the  $T_3x^4$  sandstone have similar carbon and oxygen values  
17 ( $\delta^{18}\text{O}_{\text{V-PDB}}$  -10.06 to -4.75‰, av. -7.38‰;  $\delta^{13}\text{C}_{\text{V-PDB}}$ : -0.13 to +2.46‰, av. 1.53‰)  
18 with those of carbonate rock fragments ( $\delta^{18}\text{O}_{\text{V-PDB}}$  -9.23 to -4.81‰;  $\delta^{13}\text{C}_{\text{V-PDB}}$  1.33 to  
19 +2.22‰) (Table 5, Fig. 7A). These data provide evidence for that the carbon source of  
20 the early calcite cement filling the primary pores in the  $T_3x^4$  sandstones is closely  
21 related to the internal carbonate rock fragments consisting of inorganic carbon whose  
22  $\delta^{13}\text{C}_{\text{V-PDB}}$  values can increase up to 3‰, and rarely related to the organic carbon/acid  
23 (Friedman and O' Neil, 1977). However, there was not enough acid for the dissolution  
24 of internal carbonate rock fragments at the early diagenetic stage (30-65°C). Therefore,  
25 the early calcite filling in the primary pores precipitated from pore fluids containing

1  $\text{Ca}^{2+}$  and  $\text{CO}_3^{2-}$  come from the original formation water in sandstone and adjacent  
2 mudstone at eodiagenesis stage, which were mainly related to weathering or  
3 dissolution of carbonate rock fragments in the provenance or transport process.

4 The calcite cements filling in the secondary of the  $\text{T}_3\text{x}^4$  sandstone  
5 ( $\delta^{18}\text{O}_{\text{V-PDB}}$ : -19.71‰ to -10.77‰, av. -14.69‰) pores were calculated to be precipitated  
6 at 70°C-160°C (Table 5, Fig. 19A).. The measured  $\delta^{13}\text{C}_{\text{V-PDB}}$  values (-5.43‰ ~  
7 0.75‰) show that this calcite may be related to the oxidation of organic carbon or  
8 formed under methanogenic conditions (Friedman and O'Neil, 1977; Irwin et al.,  
9 1977; Wei et al., 2015). Late-diagenetic calcite cements in the secondary pores are  
10 generally accompanied by the dissolution of feldspars and some rock fragments (e.g.  
11 carbonate rock and volcanic rock fragments)(Fig. 6D~F). Therefore, material sources  
12 of the calcite cements filling in the secondary pores is closely related to the late  
13 dissolution caused by organic acids from thermal evolution of organic matter in the  
14 source rocks. In addition, the transformation of clay minerals may also supplied some  
15  $\text{Ca}^{2+}$ ,  $\text{Fe}^{2+}$  and  $\text{Mg}^{2+}$  at the temperature range of 80°C to 140°C.

16 The  $\delta^{13}\text{C}_{\text{V-PDB}}$  values (-0.97‰ ~ +1.97‰) of the small amounts of dolomite  
17 (ankerite) filling in the secondary pores are somewhat less than those of carbonate  
18 rock fragments in the  $\text{T}_3\text{x}^4$  sandstones (Fig. 7A) and more than those of organic  
19 carbon. This suggests that the carbon source of dolomite cement may be the mixture  
20 of organic carbon and carbonate rock fragments. In addition, the relatively high  
21 precipitation temperature (75°C-140°C) (Table 5, Fig. 19B) of dolomite (ankerite)  
22 cements is consistent with the temperature of release of organic acid and  $\text{CO}_2$  from the  
23 source rock within  $\text{T}_3\text{x}^3$  and  $\text{T}_3\text{x}^5$  (Fig. 2) (Surdam et al, 1989; Zeng et al, 2007).  
24 Besides, the polycrystalline dolomite (ankerite) (30µm~80µm) generally occurs as  
25 partial replacements of detrital grains (e.g. carbonate rock fragments) and accompany

1 the dissolution of carbonate rock fragments (Fig. 6D). Therefore, the dolomite  
2 (ankerite) cements within the  $T_3x^4$  sandstones may have mainly precipitated from the  
3 dissolution of carbonate rock fragments by organic acids during mesodiagenetic stage  
4 ( $75^\circ\text{C}$ - $140^\circ\text{C}$ ).

5 In the  $T_3x^2$  sandstones, the relatively positive  $\delta^{13}\text{C}_{\text{V-PDB}}$  values ( $-1.81\%$  to  
6  $+4.97\%$ ) suggest that these carbonate cements (calcite and dolomite) were mainly  
7 formed under methanogenic conditions (Table 6, Fig. 7B) (Irwin et al., 1977; Wei et  
8 al., 2015). The calcite and dolomite cements precipitated at  $70^\circ\text{C}$ - $120^\circ\text{C}$  and  $80^\circ\text{C}$ - $160^\circ\text{C}$   
9 respectively (Table 6, Fig. 20A), which were equivalent to the mesodiagenetic stage.  
10 Concurrently, the source rock in the lower submember of  $T_3x^2$  and the underlying  
11 Xiaotangzi Formation ( $T_3x^1$ ) exists under methanogenic conditions. Carbonate  
12 cements have mainly developed in the lower submember of the  $T_3x^2$ , which is  
13 adjacent to the underlying Xiaotangzi Formation, which consists of marine source  
14 rocks (Fig. 2, Liu et al, 2014b; Luo, 2015), which can be explained by the fact that the  
15 organic acid within mudstone intruded into the sandstone. Therefore, carbon sources  
16 of carbonate cements (late diagenetic carbonate cements) in the  $T_3x^2$  could have come  
17 from the organic acids that flowed into sandstone from the source rock. The  $\text{Ca}^{2+}$ ,  
18  $\text{Fe}^{2+}$  and  $\text{Mg}^{2+}$  may come from late dissolution of feldspar and rock fragments,  
19 transformation and interstitial water of clay minerals and reduction of iron oxides.

#### 20 **5.2.2 Source, temperature and time of authigenic quartz**

21 Quartz cements are usually accompanied by sutured (microstylolitic) contacts of  
22 quartz grains formed by pressure dissolution (Fig. 8A, Fig. 8I), and increasing quartz  
23 cement content with increasing detrital quartz content in the  $T_3x^2$  sandstones (Fig. 9).  
24 However, pressure dissolution is rare in the  $T_3x^4$  sandstones, due to their low contents  
25 of detrital quartz grains. Therefore, pressure dissolution represents the most important

1 silica source for quartz cement in the  $T_3x^2$  sandstones (Luo et al., 2015), but not in the  
2  $T_3x^4$  sandstones.

3 The isolated pore-filling authigenic quartz crystals are generally accompanied by  
4 the dissolution of feldspar in the  $T_3x^2$  and  $T_3x^4$  sandstones (Fig. 8G-H). Therefore,  
5 feldspar dissolution, which was pervasive and might occur from eodiagenesis to  
6 mesodiagenesis stage (60°C-140°C), may be an important source for the quartz  
7 cements. The 80°C ~120°C is the ideal temperature range for feldspar dissolution  
8 (Surdam et al., 1989). The homogenization temperatures range (90°C and 120°C) of  
9 fluid inclusions in quartz cements of the  $T_3x^4$  sandstones (Fig. 10A) also suggest that  
10 the quartz cements may be mainly derived from the feldspar dissolution the  $T_3x^4$   
11 sandstones. However, the homogenization temperature range (90°C and 110°C) in the  
12  $T_3x^2$  sandstones are nearly absent (Fig. 9B). Moreover, the higher residual feldspar  
13 content of the  $T_3x^2$  sandstones (av. 8.3 vol%) than the  $T_3x^4$  sandstones (av. 2.1 vol%)  
14 (Table 1, Table 2, Table 3, Fig. 3A-B) and the less secondary pores of the  $T_3x^2$   
15 sandstones than the  $T_3x^4$  (Fig. 17) may also indicate that feldspar dissolution may be  
16 not the most important silica source for the quartz cements in the  $T_3x^2$  sandstones.

17 The type and content of clay minerals suggest that extensive clay mineral  
18 transformation occurred in the  $T_3x^2$  and  $T_3x^4$  sandstones (Table 2, Table 3). The nested  
19 illites related to feldspar dissolution (Fig. 11A, B, E, F), non-nested aggregates  
20 related to the illitization of smectite (Fig. 11C, O), some filamentous illites  
21 transformed from booklet-like pseudo-hexagonal kaolinite (Fig. 11N) and chlorite rim  
22 (Fig. 11G-K) were the results of clay mineral transformation. Symbiotic relationship  
23 of quartz cement and authigenic clay minerals indicates that the clay mineral  
24 transformation is the potential source for quartz cements (e. g. illite and chlorite) (Fig.  
25 8E, Fig. 11I). Moreover, the homogenization temperatures range (110°C to 140°C) of

1 quartz cements (Fig. 10A-B) is in favour of the clay minerals transformation (Worden  
2 and Morad, 2003). These indicate that clay mineral transformation within the  
3 sandstone might be one of silica sources for quartz cements in the  $T_{3x^2}$  and  $T_{3x^4}$   
4 sandstones.

5 Quartz cements with homogenization temperatures between 50°C and 90°C  
6 comprise 40% of total  $T_{3x^2}$  sandstone samples, but represent just 5% of total  $T_{3x^4}$   
7 sandstone samples (Fig. 10A, B). However, the feldspar dissolution of  $T_{3x^4}$  sandstone  
8 is more pervasive than the  $T_{3x^2}$  sandstones indicate that (Fig. 16, Fig. 17).  
9 Furthermore, some authigenic quartz located in fractures have homogenization  
10 temperatures varying from 50°C to 60°C in the  $T_{3x^2}$  sandstones. Therefore, the  
11 external silica source at eodiagenesis stage (50-60°C), which might be related to the  
12 oversaturated fluid derived from mudrocks through fractures, may be one of  
13 important silica sources for quartz cement in sandstones, especially in the  $T_{3x^2}$   
14 sandstones (Gluyas and Coleman, 1992; Gluyas et al, 2000; Luo et al., 2015).

15 In addition, the presence of some quartz cement filling in fractures with  
16 homogenization temperatures ranging from 210°C to 290°C suggests that hot fluids  
17 moving up through fractures could represent another possible external source.  
18 However, the homogenization temperatures of the quartz cements filling these pores  
19 rarely reach 200°C, which may indicate that hydrothermal fluids with high  
20 temperatures and concentrations was not an important silica source for quartz cements  
21 in the  $T_{3x^2}$  and  $T_{3x^4}$  sandstones.

### 22 **5.2.3 Temperature and time of clay mineral transformation**

23 Clay-mineral assemblages generally transform with increasing temperatures,  
24 producing a series of prograde diagenetic reactions (Worden and Morad, 2003). Clay  
25 mineral transformations in the studied sandstones include kaolinitization and

1 illitization of feldspar (Fig. 11F, M), illitization and chloritization of smectite (Fig.  
2 11O), conversion of kaolinite into illite and chlorite (Fig. 11-N), and replacement of  
3 rock fragments by mesogenetic illite and chlorite (Fig. 11B, E, J).

4 The illitization of kaolinite is prevalent at temperatures greater than  
5 approximately 70°C, but becomes pervasive at temperatures greater than  
6 approximately 130°C in neutral or alkaline environments (Worden and Morad, 2003).  
7 When the temperature is above 120-140°C, the early kaolinite released by the feldspar  
8 dissolution can be translated into illite with the K<sup>+</sup> from the K-feldspar dissolution  
9 (Chuhan and Bjørlykke, 2000; Zhang, 2011).

10 The nested illites and kaolinite are related to feldspar dissolution in the T<sub>3x</sub><sup>2</sup> and  
11 T<sub>3x</sub><sup>4</sup> sandstones (Fig. 11A, F, M, Fig. 14, Fig. 16). The K-feldspar contents have  
12 negative correlations with contents of illite (in whole rock and clay minerals) but  
13 positive correlations with chlorite in T<sub>3x</sub><sup>2</sup> sandstones (Fig. 12, Fig. 21E-F). Almost all  
14 the feldspar had been dissolved in T<sub>3x</sub><sup>4</sup> sandstones (Table 3, Fig. 13). The relative  
15 contents of kaolinite decrease with increasing content of illite and chlorite in the clay  
16 minerals of T<sub>3x</sub><sup>4</sup> sandstone (Fig. 13, Fig. 22F-J). The K<sub>2</sub>O contents have positive  
17 correlations with illite contents (in whole rock but not clay minerals) in T<sub>3x</sub><sup>2</sup> and T<sub>3x</sub><sup>4</sup>  
18 sandstones (Fig. 21J-K, Fig. 22D-E). The illitization of potassium feldspar is widely  
19 observed in the T<sub>3x</sub><sup>2</sup> sandstone and T<sub>3x</sub><sup>4</sup> sandstone (Fig. 11A, F, M). These indicate  
20 that K-feldspar dissolution coincided with, and provided the necessary K<sup>+</sup> and  
21 kaolinite for, the illitization of kaolinite in the T<sub>3x</sub><sup>2</sup> and T<sub>3x</sub><sup>4</sup> sandstones (Fig. 21E-H,  
22 Fig. 22D-F).

23 Therefore, the kaolinite formed by feldspar  
24 dissolution have generally transformed into the illite or chlorite (Fig. 11N) at the  
25 mesodiagenetic stage with deep burial (Fig. 12, Fig. 13) (Worden and Morad, 2003,



1 Chuhanand Bjørlykke, 2000; Zhang, 2011). However, the pervasive kaolinite on the  
2 top of  $T_3x^4$  formed by the dissolution and kaolinitization of feldspar (Fig. 11M), was  
3 preserved in the relatively deep burial depth (3000-4000 m) (Fig. 13, Fig. 14). This  
4 might be related to acidic condition due to top unconformity (Morad et al., 2000;  
5 Worden and Morad, 2003; Mansurbeg et al., 2006; El-ghali et al., 2006; Morad et al.,  
6 2012).

7 Almost all smectite has been transformed to illite or chlorite with the deep burial  
8 and heating of the  $T_3x^2$  and  $T_3x^4$  sandstones (Fig. 11O) (Table 2, Table 3). The  
9 negative correlation between K-feldspar and illite (Fig. 12) suggests that dissolution  
10 of K-feldspars might provide  $K^+$  for illitization of smectite. Thus, some illite  
11 occurring as non-netted aggregates may have formed by the illitization of smectite  
12 and the dissolution of K-feldspars.

13 The chloritization of smectite is a dissolution–reprecipitation process that  
14 requires a pH-alkaline fluid and a source of aluminium, iron and magnesium, which  
15 may come from the alkaline dissolution of basic volcanic fragments (Chang et al.,  
16 1986). The early authigenic chlorite rims, which mostly occurs in the middle and  
17 lower part of  $T_3x^2$  sandstones, increase with increasing K-feldspar content and  
18 decreasing illite content (Fig. 21I), indicate that chloritization was related to alkaline  
19 environment but not acidic dissolution of K-feldspar. The  $T_3x^2$  sandstones contain  
20 relatively more volcanic fragments than the  $T_3x^4$  sandstones and are adjacent to the  
21 Xiaotangzi Formation (equivalent to  $T_3x^1$ ) (Fig. 2), which was deposited in a marine  
22 environment and is characterized by slightly alkaline waters (i.e., seawater pH is 8.3)  
23 (Worden and Morad, 2003). Besides, some chlorite occurs as replacement of volcanic  
24 rock fragment accompanying by the dissolution of rock fragments (Fig. 11J, K).  
25 Therefore, early authigenic chlorite rims of  $T_3x^2$  sandstones were mainly formed by

1 the chloritization of eogenetic smectite (Fig. 12C) at eogenetic stage. Meanwhile, the  
2 alkaline dissolution of volcanic rock fragment provided the  $Mg^{2+}$  and  $Fe^{2+}$  for  
3 chloritization.

4 The pore-filling chlorite in the  $T_3x^4$  sandstones, increase with decreasing  
5 kaolinite content and increasing illite content (Fig. 22H). These pore-filling chlorites  
6 may be related to the subsequent chloritization of kaolinite at eodiagenesis and early  
7 mesodiagenesis (Fig. 13C, Fig. 22G). The early acidic dissolution of volcanic rock  
8 fragment and feldspar provides the  $Mg^{2+}$ ,  $Fe^{2+}$  and kaolinite for chloritization of  
9 kaolinite.

### 10 **5.3 Mechanism and time of compaction**

11 Compaction is the most important factor controlling the reservoir quality of the  
12 Xujiahe Formation sandstones (Huang et al., 2009; Meng et al., 2013). Although the  
13 burial depths of the  $T_3x^2$  and  $T_3x^4$  sandstones differ by approximately 1000 m,  
14 differences of degree in mechanical compaction are not so obvious, and even the  
15 mechanical compaction in the  $T_3x^4$  sandstones is stronger than that in the deeper  
16  $T_3x^2$  sandstones (Fig. 4). Moreover, the pressure dissolution (chemical compaction),  
17 which generally occur at late mesodiagenesis, is more prevalent in  $T_3x^2$  than it is in  
18  $T_3x^4$ . This abnormal phenomena can be interpreted by these facts: first, the  
19 abundances of rock fragments (25%–75%, av. 40.8 vol %) are always higher in  $T_3x^4$   
20 sandstones than they are (17%–30%, av. 21.7 vol %) in  $T_3x^2$  sandstones (Table 1);  
21 second, the early chlorite rim, which plays an important role in the preservation of  
22 primary pores, is distributed mostly in the  $T_3x^2$  sandstones but rarely in  $T_3x^4$ ; third, the  
23  $T_3x^2$  sandstones contain significantly more detrital quartz (63.3–80%, av. 70 vol%)  
24 than  $T_3x^4$  (quartz, 25–70%, av. 57.1 vol %) (Table 1). These may play an important  
25 role in the fact that the  $T_3x^2$  sandstone have more primary pore (av. 0.84%) and less

1 secondary dissolved pore (av.0.79%) than the  $T_3x^4$  sandstone (secondary pore:  
2 av.3.49%, primary pore: av.0.58%) (Fig. 17).

### 3 **5.4 Diagenetic sequence and porosity evolution**

4 Petrographic evidence observed in thin section, scanning electron microscope  
5 (SEM) and cathodoluminescence (CL) analysis can be used to decipher the relative  
6 diagenetic sequence in the study area. Moreover, the formation temperatures of  
7 authigenic minerals, which can be measured from aqueous inclusions or calculated  
8 using oxygen isotopic values can be used to infer a more accurate relative timing of  
9 the different diagenetic reactions. In summary, synthesizing petrographic observations,  
10 homogenization temperatures of fluid inclusions, isotopic analysis and source and  
11 mechanism of diagenesis can reconstruct the diagenetic history of the  $T_3x^2$  and  $T_3x^4$   
12 tight sandstones, which is illustrated in Fig. 23 and Fig. 24, in which the burial and  
13 thermal histories are based on the results of previous studies (Zhang et al., 2002).  
14 On the basis of the diagenetic sequence and previous studies, which indicate the  
15 timing of tightness of  $T_3x^2$  and  $T_3x^4$  sandstones (Luo, 2015), the porosity evolution of  
16 the  $T_3x^2$  and  $T_3x^4$  tight sandstones were reconstructed in Fig. 23 and Fig. 24.

### 17 **5.5 The characteristics, evolution and controlling factors of diagenetic** 18 **(geochemical) system**

#### 19 **5.5.1 Mass balance/transfer and evolution of diagenetic (geochemical) system**

20 The  $K_2O$  content has a weakly positive correlation with absolute and relative  
21 content of illite (in whole rock and clay minerals) in the  $T_3x^2$  sandstones (Fig. 21G-H)  
22 and but obviously positive correlation with absolute content of illite (in whole rock  
23 but not clay minerals) in the  $T_3x^4$  sandstone (Fig. 22D-E). Besides, the  $K_2O$  content  
24 was nearly stable in the vertical profile of  $T_3x^2$  sandstone but changeable in the  
25 vertical profile of  $T_3x^4$  sandstone (Fig. 12, Fig. 13). The  $K_2O$  content should be

1 controlled by the fixed composition of parent rock but not the authigenetic illite (in  
2 whole rock) in a closed sandstone system without loss and export of  $K^+$ . Furthermore,  
3 the previous research suggests that the  $T_3x^4$  have exported abundant  $K^+$ , but the  $T_3x^2$   
4 slightly exported  $K^+$  (Shen et al., 2010). These suggest that the K-feldspar  
5 dissolution provided the  $K^+$  for subsequent illitization with abundant loss of  $K^+$  in the  
6  $T_3x^4$  and little loss of  $K^+$  in  $T_3x^2$  sandstone systems at the early diagenetic stage  
7 (eodiagenesis and early mesodiagenesis) (Fig. 25A, B).

8 The dissolution of volcanic rock fragment provided the  $Mg^{2+}$  and  $Fe^{2+}$  for  
9 chloritization and dolomite cementation in  $T_3x^2$  and  $T_3x^4$  sandstone. The MgO content  
10 has a negative correlation with absolute content of chlorite (in whole rock) but a very  
11 weak negative correlation with relative content of chlorite (in clay minerals) in the  
12  $T_3x^4$  sandstone, which indicate the dissolution of volcanic rock fragment provided  
13  $Mg^{2+}$  for authigenetic chlorite with significant loss of  $Mg^{2+}$  in an open system at early  
14 diagenetic system (Fig. 24, Fig. 25A). The MgO content has a weak correlation with  
15 absolute content of chlorite (in whole rock) but a negative correlation with relative  
16 content of chlorite (in clay minerals) in the  $T_3x^2$  sandstones (Fig. 21B-C), which  
17 indicate alkaline dissolution of volcanic rock fragment provided  $Mg^{2+}$  for the early  
18 authigenetic chlorite with little loss of  $Mg^{2+}$  at early diagenetic stage (Fig. 23, Fig.  
19 25B). The content of MgO (in whole rock) increase with the increasing dolomite (in  
20 whole rock) in the  $T_3x^2$  and  $T_3x^4$  sandstone (Fig. 21A, Fig. 22A), which suggests that  
21 the dissolution of volcanic rock fragment provided all the  $Mg^{2+}$  for the dolomite  
22 cement without significant export of  $Mg^{2+}$  at mesodiagenesis in the  $T_3x^2$  and  $T_3x^4$   
23 closed sandstone system (Fig. 25A, B).

24 The contents of  $K_2O$ , MgO,  $Al_2O_3$  in  $T_3x^4$  sandstone have more obvious vertical  
25 changes than  $T_3x^2$  sandstone (Fig. 12, Fig. 13). Moreover, feldspar dissolution and

1 related secondary pores in the  $T_3x^4$  sandstone are obviously more pervasive than  $T_3x^2$   
2 sandstone (Fig. 15, Fig. 16, Fig.17, Table 2, Table 3). However, the content of quartz  
3 cement in  $T_3x^4$  sandstone (av.0.94%) is obvious less than  $T_3x^2$  sandstone  
4 (av.2.16%)(Table 1).Fig. 15These indicate that the  $T_3x^4$  sandstone has ever  
5 experienced a more open geochemical system than  $T_3x^2$  sandstone during the feldspar  
6 dissolution process at the eodiagenesis and early mesodiagenesis (Fig. 25A, B).  
7 Besides, the large amount of factures, enlarged dissolution of the micro-fractures and  
8 some quartz cement filling in fractures indicate that the focused fluid flow on  
9 fractures also represent partially more open systems during burial process in  $T_3x^4$   
10 sandstone and  $T_3x^2$  sandstone (Fig. 15F, Fig. 25) (Zhang, 2005; Zeng, 2010; Luo,2015;  
11 Bjørlykke and Jahren, 2012).

### 12 **5.5.2 Controlling factors on the diagenetic (geochemical) system**

13 The deltaic setting and subsequent uplift and development of an unconformity  
14 controlled the early digenetic history of the sandstones when at shallow burial depth.  
15 Subsequent deep burial depth and tectonism drove the diagenetic alterations in the  
16 tight sandstone diagenesis system, because they accelerated diagenetic alterations by  
17 increasing the formation pressure and paleotemperature and produced abundant  
18 fractures (Fig. 23, Fig. 24).

### 19 **5.2.3 Impacts on the reservoir quality of diagenetic (geochemical) system**

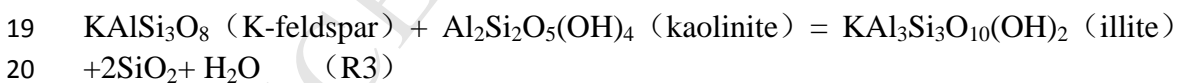
20 Diagenetic modifications alter the types, amount and distribution of pore spaces,  
21 creating smaller and more disconnected pores (Lai et al., 2018a; Lai et al., 2018b).  
22 The diagenetic reactions, particularly the dissolution, generally result in significant  
23 changes in the sediment composition (e.g.  $K^+$ ,  $Mg^{2+}$  and silica) (Fig. 12, Fig. 13, Fig.  
24 21, Fig. 22) and formation of secondary pores in the open diagenetic (geochemical)  
25 system during near-surface , eodiagenesis and even early mesodiagenesis stage (Fig.

1 16, Fig. 17, Fig. 23, Fig. 24, Fig. 25A-B).. Besides, the  $T_3x^4$  sandstone has ever  
 2 experienced a more open geochemical system than  $T_3x^2$  sandstone at the eodiagenesis  
 3 and early mesodiagenesis (Fig. 25A, B). Therefore, the  $T_3x^4$  sandstone produced more  
 4 early calcite cements, kaolinite and secondary pores than  $T_3x^2$  sandstone in the open  
 5 diagenetic system at eodiagenesis and early mesodiagenesis (Fig. 15, Fig.17, Table 1,  
 6 Table 2).

7 When the geotemperature is above 120-140°C that determined by burial depth,  
 8 the early kaolinite released by the feldspar dissolution can translated into the illite  
 9 with the  $K^+$  from the K-feldspar dissolution (R1 and R2), which can merge into one  
 10 reaction (R3) (Chuhan et al., 2000; Zhang, 2011). The little amount of residual acids at  
 11 eodiagenesis stage can trigger the illitization of K-feldspar (R3). Hence, the  
 12 illitization of K-feldspar were controlled by the relative ratio of K-feldspar to  
 13 kaolinite in closed geochemical system (Chuhan and Bjørlykke, 2000; Huang et al.,  
 14 2009). The reaction for illitization of K-feldspar (R3) will produce 10.7% secondary  
 15 space volume (Huang et al., 2009).



18



21 The ratio of kaolinite to K-feldspar in the  $T_3x^4$  sandstone exceeded 1, so almost  
 22 all the K-feldspar and part of kaolinite had translated into illite (Table 3). Whereas,  
 23 the ratio of kaolinite to K-feldspar in the  $T_3x^2$  was less than 1, so almost all the  
 24 kaolinite and part of K-feldspar had translated into illite (Table 2) (Chuhan and  
 25 Bjørlykke, 2000). Consequently, the illitization of K-feldspar (R3) in the  $T_3x^4$   
 26 sandstone produced more secondary pores than  $T_3x^2$  sandstone in closed geochemical  
 27 system during mesodiagenesis (Fig. 25).

1        The strong mechanical and chemical compaction (pressure dissolution) of the  
2  $T_3x^2$  and  $T_3x^4$  tight sandstone destroyed most of the primary pores and some  
3 secondary pores (Fig. 4, Fig. 25A-B). The early secondary pore formed in open  
4 system may be destroyed by subsequent compaction. However, the associate kaolinite,  
5 which was generally formed by early feldspar dissolution in open system, will  
6 determine the late effective secondary pores by influencing late illitization of  
7 K-feldspar (R3) at mesodiagenesis (Fig. 25). Therefore, the average secondary  
8 thin-section porosity of  $T_3x^4$  sandstone (av.3.49) is obviously higher than  $T_3x^2$   
9 sandstone (av.0.79%) (Fig. 4). The average primary porosity of  $T_3x^2$  sandstone  
10 (av.1.09%) is higher than the  $T_3x^4$  sandstone(av.0.58%), because grain-coating clay  
11 minerals (chlorite rim and illite coating) of  $T_3x^2$  sandstone help to preserve porosity at  
12 depth by retarding compaction in the relatively closed system (Fig.11I,K, Fig. 25)(Luo  
13 et al.,2019). However, the pore space was dominated by secondary dissolution pores  
14 in the  $T_3x^2$  sandstone and  $T_3x^4$  sandstone, and both core porosity and permeability of  
15  $T_3x^4$  sandstone are therefore obviously higher than the  $T_3x^2$  sandstone (Fig. 18, Fig.  
16 25). The late diagenesis (late carbonate and quartz cementation) of the  $T_3x^2$  and  $T_3x^4$   
17 sandstone, which were related to the dissolution and precipitation, produce no  
18 significant change of composition and porosity in nearly closed system at the late  
19 diagenetic stage. Therefore, the diagenetic characteristics and evolution of diagenetic  
20 systems can be used to predict about the reservoir quality based on the burial history,  
21 tectonic activities and certain primary sediment composition related to delta facies  
22 and provenance (Fig. 25A-B).

## 23 **6. Conclusions**

24        This study of the upper Triassic Xujiahe Formation in the Western Sichuan  
25 foreland basin, China, yields important clues about the diagenetic characteristics, size,

1 evolution and controlling factors of the diagenetic (geochemical) system and their  
2 impacts on reservoir quality in the tight deltaic sandstone, including the following:

3 1. Tight deltaic sandstones have undergone a significant and complicated series  
4 of diagenetic modification.

5 2. The strong compaction and carbonate cementation destroyed almost all the  
6 primary pores. The feldspar dissolution was the most important source of pore space  
7 in the  $T_3x^2$  and  $T_3x^4$  sandstones.

8 3. The  $T_3x^4$  sandstone with significant loss of  $K^+$ ,  $Mg^{2+}$  and silica experienced a  
9 more open diagenetic (geochemical) system than the  $T_3x^2$  sandstone at near-surface,  
10 eodiagenesis and early mesodiagenesis stage.

11 4. The  $T_3x^4$  sandstone produced more early calcite cements, kaolinite and  
12 secondary pores than  $T_3x^2$  sandstone in the open diagenetic system at eodiagenesis  
13 and early mesodiagenesis (Fig. 4, Fig.16, Table 1, Table 2).

14 5. Both the  $T_3x^2$  and  $T_3x^4$  sandstone represent nearly closed diagenetic  
15 (geochemical) system during middle-late mesodiagenesis. The late dissolution and  
16 illitization of K-feldspar, which was controlled by the parent composition (e.g.  
17 K-feldspar) and diagenesis in early open system (e.g. remaining kaolinite,  $K^+$ ,  
18 K-feldspar and acids), was the main pore sources in the closed system.

## 19 **7. Acknowledgements**

20 The authors gratefully thank the editor and the reviewers for their valuable  
21 comments. Moreover, we specially thank Research Institute of Petroleum Exploration  
22 & Development, Southwest Oil-Gas Branch Company of Sinopec for providing all the  
23 related core samples and geological data. This study was jointly supported by the  
24 Major Special Project for National Science and Technology [Grant numbers.



1 2016ZX05033-001-002], the National Natural science Foundation of China [Grant  
2 numbers. 41202043] and the China Scholarship Council (CSC).

### 3 **References**

4 Bjørlykke, K., 2010, Petroleum geoscience: From sedimentary environments to rock physics: New  
5 York, Springer Verlag, 508 .

6 Bjørlykke, K., 2011. Open-system chemical behaviour of Wilcox Group mudstones. How is large  
7 scale mass transfer at great burial depth in sedimentary basins possible? A discussion. Mar.  
8 Petrol. Geol. 28, 1381–1382.

9 Bjørlykke, K., 2014. Relationship between depositional environments, burial history and rock  
10 properties. Some principal aspects of diagenetic process in sedimentary basins. Sediment.  
11 Geol. 301, 1-14.

12 Bjørlykke, K., Jahren, J., 2012. Open or closed geochemical systems during diagenesis  
13 insedimentary basins: constraints on mass transfer during diagenesis and the prediction of  
14 porosity in sandstone and carbonate reservoirs. AAPG Bull. 96, 2193–2214.

15 Boles, J, R., Franks, S, G., 1979. Clay diagenesis in Wilcox sandstones of southwest  
16 Texas: implications of smectite diagenesis on sandstone cementation. J. Sediment Petrology. 49,  
17 55-70.

18 Chang, H.K., Mackenzie, F.T. Schoonmaker, J., 1986. Comparisons between the diagenesis of  
19 dioctahedral and trioctahedral smectite, Brazilian offshore basins. Clay Miner. 34, 407–423.

20 Chuhan, F.A., Bjørlykke, K., 2000. The role of provenance in illitization of deeply buried reservoir  
21 sandstones from Haltenbanken and north Viking Graben, offshore Norway. Mar. Pet. Geol. 17,  
22 673-689.

23 Clark, S.J., 2014. Constraining diagenetic timings, processes and reservoir quality in  
24 igneous-affected basins, Durham theses, Durham University. Available at Durham E-Theses  
25 Online: <http://etheses.dur.ac.uk/10827/>. Curtis, C, D., 1978. Possible link between sandstone  
26 diagenesis and depth-related geochemical reactions occurring in enclosing mudstone. J. Geol.  
27 Soc. Lond 135, 107-114.

28 Day-Stirrat, R.J., Milliken, K.L., Dutton, S.P., Loucks, R.G., Hillier, S., Aplin, A.C., Schleicher,

- 1 A.M., 2010. Open-system chemical behavior in deep Wilcox Group mudstones, Texas Gulf  
2 Coast, USA. *Mar. Pet. Geol.* 27, 1804-1818.
- 3 Day-Stirrat, R. J., K. L. Milliken, S. P. Dutton, R. G. Loucks, S. Hillier, A. C. Aplin, and A. M.  
4 Schleicher, 2011, Discussionin response to Knut Bjørlykke regarding JMPG\_1376  
5 “Open-system chemical behavior in deep Wilcox Group mudstones, Texas Gulf Coast,  
6 U.S.A”. *Mar. Pet. Geol.* 28, 1383–1384.
- 7 Dias, R. F., Freeman, K. H., Lewan, M. D., Franks, S. G., 2002.  $\delta^{13}\text{C}$  of low-molecular weight  
8 organic acids generated by the hydrous pyrolysis of oil-prone source rocks. *Geochimica*  
9 *Cosmochimica Acta.* 66 (15), 2755–2769.
- 10 El-Ghali,M,A,K., El Khoriby,E,, Mansurbeg,H., Morad,S., Ogle,N.,2013., Distribution of  
11 carbonate cements within depositional facies and sequence stratigraphic framework of  
12 shoreface and deltaic arenites,Lower Miocene, the Gulf of Suez rift, Egypt .*Mar. Pet. Geol.*45,  
13 267-280.
- 14 El-ghali,M,A,K., Tajori,K,G., Mansurbeg,H.,2006. The influence of transgression and regression  
15 on the spatial and temporal distribution of diagenetic kaolin in the Upper Ordovician  
16 glaciogenic sandstones within a sequence stratigraphic framework, Murzuq Basin, SW Libya.  
17 *J. Geochem. Explor.*89, 87-91.
- 18 Friedman, I., O’Neil, J.R., 1977. *Data of Geochemistry: Compilation of Stable Isotope*  
19 *Fractionation Factors of Geochemical Interest [M].* US Government Printing Office.
- 20 Folk, R. L., 1980. *Petrology of Sedimentary Rocks.* Hemphill Publishing Co., Austin, Texas.
- 21 Gier, S., Worden, H.R., Johns, D.W., Kurzweil, H., 2008. Diagenesis and reservoir quality of  
22 Miocene sandstones in the Vienna Austria. *Mar. Petrol.Geol.* 25,681-695.
- 23 Gluyas, J., Coleman, M., 1992. Material flux and porosity changes during sediment diagenesis  
24 *Nature:* 356, 52-54.
- 25 Gluyas, J.G.,1997. Poroperm Prediction for Reserves Growth Exploration: Ula Trend Norwegian  
26 North Sea, AAPG Memoir 69, 201-210.
- 27 Gluyas, J. G., Witton, T., 1997. Poroperm prediction for wildcat exploration prospects, Miocene  
28 Southern Red Sea, AAPG Memoir, 69, 163-176.
- 29 Gluyas, J.G., Garland, C.R., Oxtoby, N.H. and Hogg, A.J.C. (2000) Quartz cement; the Miller's

- 1 tale In Special Proceedings Vol 29, International Association of Sedimentologists (eds R.  
2 H. Worden and S Morad) 199-219
- 3 Hansen, H, N., Løvstad, K., Müller, R., Jahren, J., 2017. Clay coating preserving high porosities in  
4 deeply buried intervals of the Stø Formation. *Mar. Pet. Geol.* 88, 648-658.
- 5 Hawkins, P.J., 1978. Relationship between diagenesis, porosity reduction, and oil emplacement in  
6 late Carboniferous sandstone reservoirs, Bothamsall oilfield, east Midlands. *Journal of*  
7 *Geological Society.* 135, 7–24.
- 8 Huang, S., Huang, K., Feng, L., Tong, H., Liu, L., Zhang, X., 2009. Mass exchanges among feldspar,  
9 kaolinite and illite and their influences on secondary porosity formation in clastic  
10 diagenesis—A case study on the Upper Paleozoic, Ordos basin and Xujiahe Formation, Western  
11 Sichuan depression. *Geochimica.* 38(05), 498-506 (in Chinese with English Abstract).
- 12 Irwin, H., Curtis, C., Coleman, M., 1977. Isotopic evidence for source of diagenetic carbonates  
13 formed during burial of organic-rich sediments. *Nature.* 269, 209–213.
- 14 Kaus, K.G., Copenhaver, S.A., Braun, R.L., Burnham, A.K., 1997. Hydrous pyrolysis of New  
15 Albany and Phosphoria Shales: production kinetics of carboxylic acid and light hydrocarbons  
16 and interactions between the inorganic and organic chemical systems. *Org. Geochem.* 27  
17 (7/8), 477–496.
- 18 Lai, J., G. Wang, Y. Ran, and Z. Zhou, 2015, Predictive distribution of high quality reservoirs of  
19 tight gas sandstones by linking diagenesis to depositional facies: Evidences from Xu-2  
20 sandstones in Penglai area of central Sichuan basin, China. *J. Nat. Gas. Sci. Eng.* 23, 97–111.
- 21 Lai, J., Wang, G., Wang, Z., Chen, J., Pang, X., Wang, S., Zhou, Z., He, Z., Qin, Z., Fan, X., 2018a.  
22 A review on pore structure characterization in tight sandstones: *Earth Sci. Rev.* 177, 436-457.
- 23 Lai, J., Wang, G., Cao, J., Xiao, C., Wang, S., Pang, X., Dai, Q., He, Z., Fan, X., Yang, L., Qin,  
24 Z., 2018b. Investigation of pore structure and petrophysical property in tight sandstones. *Mar.*  
25 *Pet. Geol.* 91, 179-189.
- 26 Lin, L., 2005. Sedimentary Facies and Paleogeographic Evolution of the upper Triassic Xujiahe  
27 Formation in West Sichuan Foreland. (master thesis) Chengdu university of technology,  
28 Chengdu, Sichuan, China. 21-40 (in Chinese with English Abstract).
- 29 Liu, S., 2010. Research on Origin of Fluid and Gas Dynamic Accumulation Characteristics of

- 1 Xujiahe Formation in the Middle Member of West Sichuan Depression. (doctor thesis)  
2 Chengdu university of Technology, Chengdu, Sichuan, China (in Chinese with English  
3 Abstract).
- 4 Liu, S., Shen, Z., Lv, Z., Wang, P., 2014a.Characteristics and porosity evolution of relatively  
5 high-quality reservoirs of T<sub>3</sub>x<sup>4</sup> in Xinchang area, Sichuan, China. Journal. Chengdu  
6 University Technology (Science and Technology Edition).41(04), 428-436 (in Chinese with  
7 English abstract).
- 8 Liu, S., Huang, S., Shen, Z., Lv, Z., Song, R.,2014b. Diagenetic fluid evolution and water-rock  
9 interaction model of carbonate cements in sandstone: An example from the reservoir  
10 sandstone of the Fourth Member of the Xujiahe Formation of the Xiaoquan-Fenggu area,  
11 Sichuan Province, China.Science China: Earth Sci. 57, 1077–1092(in Chinese with English  
12 abstract).
- 13 Luo, L., Meng, W., Feng, M., Tan, X., Zhang, S., Sun, S., Xiao, C., 2015. Silica sources of quartz  
14 cements and its effects on the reservoir in tight sandstones: A case study on the second  
15 member of the Xujiahe Formation in Xinchang structural belt, western Si-chuan depression.  
16 Natl Gas Geosci. 26(03), 435-443(in Chinese with English abstract).
- 17 Luo, L., 2015.Research on diagenetic facies of the 2<sup>nd</sup> member of Xujiahe Formation in the  
18 Xinchang structural belt. (master thesis) Chengdu university of Technology, Chengdu,  
19 Sichuan, China (in Chinese with English Abstract).
- 20 Luo, L., Gao,X., Meng,W., Tan,X., Shao ,H., Xiao, C.,2018. The origin and alteration of calcite  
21 cement in tight sandstones of Jurassic Shishugou Group in the Fukang Sag, Junggar Basin,  
22 NW China: Implications for fluid–rock interactions and porosity evolution. Aust. J. Earth. Sci.  
23 65(3), 427-445.
- 24 Luo,L., Gao,X., Gluyas,J., Tan,X., Cheng,C., Kong,X., Qu,F., Shao,H.,2019. Reservoir quality  
25 prediction of deeply buried tight sandstones in extensively faulted region: A case from the  
26 Middle-Upper Jurassic Shishugou Group in central Junggar Basin, NW China. J. Petrol. Sci.  
27 Eng. 175, 22–45.
- 28 Luo, L., Gao, X., Meng, W., Tan, X., Feng, M., Shao, H., 2017. The Formation Mechanism of the  
29 Relatively High-quality Reservoir in Tight Sandstones with Deep Burial: A Case Study of

- 1 Xujiahe Formation in Xinchang Structural Belt of Western Sichuan Depression. *Acta*  
2 *Geoscientica Sinica*.38(6),930-944 (in Chinese with English Abstract).
- 3 Mansurbeg,H., El-ghali,M,A,K., Morad,S., Plink-Björklund,P.,2006. The impact of meteoric water  
4 on the diagenetic alterations in deep-water, marine siliciclastic turbidites. *J. Geochem.*  
5 *Explor.*89, 254-258.
- 6 Meng,W., Lv, Z., Feng,M.,Zhang,S.,Li,M.,Mai,F.,2011. The origin of authigenic illite in tight  
7 sandstones and its effect on the formation of relatively high-quality reservoirs: A case study  
8 on sandstones in the 4th member of Xujiahe Formation, western Sichuan Basin. *ACTA*  
9 *PETROLEI SINICA*.32(5), 783-790.
- 10 Meng, W., Lv, Z., Liu, J., Tian, J., Feng, M., Li M., 2013. Reservoir controlling factors and  
11 geological prediction models of the 4th member of the Xujiahe Formation in  
12 Xiaoquan-Xinchang area, the western Sichuan basin. *Oil .Gas .Geol.* 34, 483-490(in Chinese  
13 with English Abstract).
- 14 Morad, S., Al-Aasm, I.S., Nader, F.H., Ceriani, A., Gasparrini, M., Mansurbeg, H., 2012.Impact of  
15 diagenesis on the spatial and temporal distribution of reservoir quality in the Jurassic Arab D  
16 and C members, Offshore Abu Dhabi Oilfield, United Arab Emirates. *GeoArabia*17, 17-56.
- 17 Morad, S., Ketzer, J.M. De Ros, L.F., 2000. Spatial and temporal distribution of diagenetic  
18 alterations in siliciclastic rocks: implications for mass transfer in sedimentary basins.  
19 *Sedimentology.* 47 (Millenium Reviews), 95–120.
- 20 Ni, Y., Dai, J., Tao, S., Wu, X., Liao, F., Wu, W., Zhang, D., 2014. Helium signatures of gases  
21 from the Sichuan Basin, China. *Org Geochem.* 74, 33-43.
- 22 Shen, Z., Gong, Y., Liu S., Lv Z., 2010. A discussion on genesis of the upper Triassic Xujiahe  
23 Formation water in Xinchang area, Western Sichuan depression. *Geological Review.*  
24 56(01):82-88(in Chinese with English Abstract).
- 25 Shi, L., 2010. Research on reservoir characteristics of the second member of the Upper Triassic  
26 Xujiahe Formation in Xiaoquan-Xinchang area,Western Sichuan Depression (master thesis)  
27 Yangtze university, Wuhan, Hubei, China.27-31 (in Chinese with English Abstract).
- 28 Surdam, R.C., Crossey, L.J., Hagen, E.S. & Heasler, H.P.,1989. Organic–inorganic interactions  
29 and sandstone diagenesis. *AAPG Bull.*73, 1–23.

- 1 Tang, J., Huang, Y., Xu, X., John, T., James, H., 2009. Application of converted-wave 3D/3-C data  
2 for fracture detection in a deep tight-gas reservoir. *The leading edge*. July, 826-837.
- 3 Tao, S., Zou, C., Mi, J., Gao, X., Yang, C., Zhang, X., Fan, J., 2014. Geochemical comparison  
4 between gas in fluid inclusions and gas produced from the Upper Triassic Xujiahe Formation,  
5 Sichuan Basin, SW China. *Org. Geochem.* 74, 59-65.
- 6 Van der Plas, L., and A. C. Tobi, 1965, A chart for judging the reliability of point counting results.  
7 *American Journal of Science.* 263(1), 87–90, doi:10.2475/ajs.263.1.87.
- 8 Wang, J., 2012. The water-rock interaction mechanism of the relatively higher quality sandstone  
9 reservoirs formation in the fourth member of Xujiahe formation, Xiaoquan-FengGu  
10 area (master thesis). Chengdu University of Technology, Chengdu, Sichuan, China (in  
11 Chinese with English Abstract).
- 12 Wei, W., Zhu, X., Tan, M., Xue, M., Guo, D., Su, H., Wang, P., 2015. Diagenetic and porosity  
13 evolution of conglomerate sandstones in Bayingebi Formation of the Lower Cretaceous,  
14 Chagan Sag, China -Mongolia frontier area. *Mar. Petrol. Geol.* 66, 998-1012.
- 15 Worden, R.H., Morad, S., 2000. Quartz cementation in oil field sandstones: a review of the key  
16 controversies. In: Worden, R.H., Morad, S. (Eds.), *Quartz Cementation in Sandstones*.  
17 Wiley-Blackwell, pp. 1-20.
- 18 Worden, R.H., Morad, S., 2003. Clay minerals in sandstones: controls on formation,  
19 distribution and evolution. In: Worden, R.H., Morad, S. (Eds.), *Clay mineral cements in*  
20 *sandstones* International Association of Sedimentologists (IAS) Special Publication 34.  
21 Blackwell, UK, pp. 3–41.
- 22 Xu C., Gehenn J M., Zhao D., Xie G., Teng M K., 2015. The fluvial and lacustrine sedimentary  
23 systems and stratigraphic correlation in the Upper Triassic Xujiahe Formation in Sichuan  
24 Basin, China. *AAPG Bull.* 99, 2023–2041.
- 25 Ye, T., Zhang, H., Tang, J., 2009. Identification of high efficiency payzones with high permeability  
26 in deep fractured tight detrital reservoirs: A case study of gas reservoir in the Upper Triassic  
27 Xujiahe Formation of Xinchang gas field in western Sichuan basin. *Nat. Gas Industry* .29,  
28 22-26.
- 29 Yuan, G., Cao, Y., Yang, T., Wang, Y., Li, X., Xi, K., Jia, Z., 2013. Porosity enhancement potential

- 1 through mineral dissolution by organic acids in the diagenetic process of clastic reservoir.  
2 Earth Science Frontier. 20(5), 207-219 (in Chinese with English Abstract).
- 3 Yuan, G., Gluyas, J., Cao, Y., Oxtoby, H.N., Jia, Z., Wang, Y., 2015a. Diagenesis and reservoir  
4 quality evolution of the Eocene sandstones in the northern Dongying Sag, Bohai Bay Basin,  
5 East China. *Mar.Petrol. Geol.* 22, 77–89.
- 6 Yuan, G., Cao, Y., Gluyas, J., Li, X., Xi, K., Wang, Y., Jia, Z., Sun, P., Oxtoby, N. H.,  
7 2015b. Feldspar dissolution, authigenic clays, and quartz cements in open and closed  
8 sandstone geochemical systems during diagenesis: Typical examples from two sags in Bohai  
9 Bay Basin, East China. *AAPG Bull.* 99, 2121-2154.
- 10 Yuan, G., Cao, Y., Zhang, Y., Gluyas, J., 2017a. Diagenesis and reservoir quality of sandstones  
11 with ancient “deep” incursion of meteoric freshwater --An example in the Nanpu Sag, Bohai  
12 Bay Basin, East China. *Mar.Petrol.Geol.* 82, 444–464.
- 13 Yuan, G., Cao. Y., Qiu, L., Chen, C., 2017b. Genetic mechanism of highquality reservoirs in  
14 Permian tight fan delta conglomerates at the northwestern margin of the Junggar Basin,  
15 northwestern China: *AAPG Bulletin*. v.101, P. 1995-2019.
- 16 Zeng, J., Zhu, Z., Wu, Q., Peng, J., 2007. Experimental study on the generation of organic acids  
17 from source rocks and its effect factors. *Acta Sedimentol. Sin.* 25(6), 847-851(in Chinese  
18 with English abstract).
- 19 Zeng, L., 2010. Microfracturing in the UpperTriassic Sichuan Basin tight-gas sandstones: Tectonic,  
20 overpressure, and diagenetic origins. *AAPG Bull.* 94, 1811-1825.
- 21 Zhang, G., 2005. Characteristics of fractures in the tight sandstone reservoirs of Xujiahe  
22 Formation in west Sichuan depression. *Nat. Gas Industry.* 25(7), 11-13.(in Chinese with  
23 English abstract).
- 24 Zhang J., Chang X., Wang S., 2002. Gas trap in deep basin of the upper Triassic in Sichuan Basin.  
25 *Acta. Petrol.Sin.* 23, 27-33.
- 26 Zhang, X., 2011. The mechanism of feidspar dissolution and conservation in Upper Triassic  
27 Xujiahe Formation in Xinchang of Western Sichuan. (master thesis) Chengdu university of  
28 Technology for Master Degree, Chengdu, Sichuan, China. 35-50(in Chinese with English  
29 Abstract).

1 Zheng,J., Ying,F.,1997. Reservoir Characteristics and Diagenetic model of sandstone intercalated  
2 in Coal-Bearing Strata. ACTA PETROLEI SINICA.18(4), 19-24.

3 Zheng R., Peng J., Gao H., Ke G., 2003. Analysis of the fracture active stages,heat fluid nature  
4 and the process of Forming reservoir in western Sichuan sag. J. Chengdu University  
5 Technology (Science and Technology Edition). 30,551-558 (in Chinese with English  
6 Abstract).

7

8

9

10



**Table 1.** Petrological composition of the  $T_3x^2$  and  $T_3x^4$  sandstones in the studied area

Stratum	Quartz, %	Feldspar, %	Rock fragment, %				Carbonate cement, %		Quartz cement, %
			Sedimentary rock, %	metamorphic rock, %	Volcanic rock, %	Total, %	Calcite	Dolomite	
$T_3x^4$	<u>25.0-70.0</u> 57.1	<u>0.5-4.0</u> 2.1	29.1	8.4	3.3	<u>25.0-75.0</u> 40.8	4.97	0.95	0.94
$T_3x^2$	<u>63.3-80.0</u> 70.0	<u>3.0-13.0</u> 8.3	10.0	10.0	1.7	<u>17.0-30.0</u> 21.7	3.72	2.96	2.16

Minimum-Maximum

Average

**Table 2.** Mineral contents in the T<sub>3</sub>X<sup>2</sup> sandstones (XRD)

Well	Strata	Depth (m)	Whole rock(%)								Clay mineral(%)				
			Clay	Quartz	K-feldspar	plagioclase	Calcite	Dolomite	Illite	I/S	C/S	S/I	Smectite	Kaolinite	Chlorite
X11	T <sub>3</sub> X <sup>2</sup>	4755.72	4.8	85.2	0	8.4	0.6	0	85	0	0	0	0	0	15
X11	T <sub>3</sub> X <sup>2</sup>	4756.84	12.5	70.3	0	13.2	0	0.4	82	0	0	0	0	0	18
X11	T <sub>3</sub> X <sup>2</sup>	4757.77	8	73.9	0	16.9	0	1.2	74	0	0	0	0	0	26
X11	T <sub>3</sub> X <sup>2</sup>	4759.93	7.8	77.4	0	12.2	0	1	75	0	0	0	0	0	25
X11	T <sub>3</sub> X <sup>2</sup>	4762.66	4.4	83.7	0	11.5	0	0.4	67	0	0	0	0	0	33
X11	T <sub>3</sub> X <sup>2</sup>	4764.82	0.9	90.3	0	8.8	0	0	77	0	0	0	0	0	23
X11	T <sub>3</sub> X <sup>2</sup>	4766.62	0.01	90.3	0	9.7	0	0	73	0	0	0	0	0	27
X11	T <sub>3</sub> X <sup>2</sup>	4768.30	3.4	88.4	0	7.5	0	0.7	73	0	0	0	0	0	27
X10	T <sub>3</sub> X <sup>2</sup>	4847.63	6.4	92.1	0	0	0.4	1.1	67	0	0	0	0	0	33
X10	T <sub>3</sub> X <sup>2</sup>	4850.16	5.3	68.4	4.5	21.4	0	0.4	70	0	0	0	0	0	30
X10	T <sub>3</sub> X <sup>2</sup>	4851.34	7.1	80.2	3.4	8.3	0	1	71	0	0	0	0	0	29
X10	T <sub>3</sub> X <sup>2</sup>	4853.56	9.7	74.2	0	13.4	0	2.7	73	0	0	0	0	0	27
X10	T <sub>3</sub> X <sup>2</sup>	4855.15	2.3	80.8	3.5	10.4	0	3	73	0	0	0	0	0	27
X10	T <sub>3</sub> X <sup>2</sup>	4880.24	0.01	96.7	2	1.3	0	0	17	34	0	0	0	0	49
X10	T <sub>3</sub> X <sup>2</sup>	4924.32	2.7	73.7	8	15.4	0	0.2	24	0	0	0	0	0	76
X10	T <sub>3</sub> X <sup>2</sup>	4927.08	3.1	69.7	11.8	15.4	0	0	21	0	0	0	0	0	79
X10	T <sub>3</sub> X <sup>2</sup>	4927.83	2.7	70.1	13.3	13.6	0	0.3	24	0	0	0	0	0	76
X10	T <sub>3</sub> X <sup>2</sup>	4929.74	5	71.2	10.8	12.8	0	0.2	11	0	0	0	0	0	89
X10	T <sub>3</sub> X <sup>2</sup>	4930.19	2.3	76.3	14.1	7.2	0	0.1	20	0	0	0	0	0	80
X10	T <sub>3</sub> X <sup>2</sup>	4932.65	3	75.3	10.3	11.2	0	0.2	27	7	0	0	0	0	66
X10	T <sub>3</sub> X <sup>2</sup>	4936.12	3.9	75.4	9.3	11.4	0	0	23	0	0	0	0	0	77
X10	T <sub>3</sub> X <sup>2</sup>	4937.00	1.8	75.9	7.9	14.1	0.1	0.2	21	0	0	0	0	0	79
X11	T <sub>3</sub> X <sup>2</sup>	5018.02	7.5	68.6	10.1	13.6	0	0.2	26	0	0	0	0	0	74
X11	T <sub>3</sub> X <sup>2</sup>	5020.30	8.6	72	8.1	11.3	0	0	24	0	0	0	0	0	76
X11	T <sub>3</sub> X <sup>2</sup>	5021.53	9.6	67.7	6.5	15.5	0.3	0.4	27	0	0	0	0	0	73
X11	T <sub>3</sub> X <sup>2</sup>	5022.52	5.8	80.6	2.5	10.3	0.4	0.4	25	0	0	0	0	0	75
X11	T <sub>3</sub> X <sup>2</sup>	5064.68	6.3	78.2	8	7.1	0.1	0.3	36	0	0	0	0	0	64
X11	T <sub>3</sub> X <sup>2</sup>	5067.14	4.9	75	7.3	11.1	0.1	0	29	0	0	0	0	0	71
X11	T <sub>3</sub> X <sup>2</sup>	5070.01	4.4	76.1	10.5	8	0.8	0.2	43	0	0	0	0	0	57
X11	T <sub>3</sub> X <sup>2</sup>	5072.84	2.8	81	5	10.6	0.3	0.3	45	0	0	0	0	0	55
X11	T <sub>3</sub> X <sup>2</sup>	5075.64	1.3	76.5	6.6	15.3	0.3	0	48	0	0	0	0	0	52
X11	T <sub>3</sub> X <sup>2</sup>	5078.00	7.8	74.1	4.5	12.3	0.7	0.6	48	0	0	0	0	0	52
	<b>Average</b>		4.9	77.8	5.3	11.3	0.2	0.5	46.8	1.3	0	0	0	0	51.9

**Table 3.** Mineral contents in the T<sub>3</sub>x<sup>4</sup> sandstones (XRD)

Well	Strata	Depth (m)	Whole rock (%)								Clay mineral (%)				
			Clay mineral	Quartz	K-feldspar	plagioclase	Calcite	Dolomite	Illite	I/S	C/S	S/I	Smectite	Kaolinite	Chlorite
X11	T <sub>3</sub> x <sup>4</sup>	3466.57	4.5	92.3	0	0	3.2	0	55	0	0	0	0	27	18
X11	T <sub>3</sub> x <sup>4</sup>	3468.31	4.9	94.3	0	0	0.7	0.1	49	0	0	0	0	26	25
X11	T <sub>3</sub> x <sup>4</sup>	3470.64	11.1	88.2	0	0	0.7	0	41	0	0	0	0	24	35
X11	T <sub>3</sub> x <sup>4</sup>	3472.00	11.3	88.3	0	0	0	0.4	44	0	0	0	0	17	39
X11	T <sub>3</sub> x <sup>4</sup>	3474.12	12.4	86.1	0	1	0.2	0.3	41	12	0	0	0	32	15
X11	T <sub>3</sub> x <sup>4</sup>	3475.67	1.6	96.5	0	0	1.9	0	58	0	0	0	0	0	42
X11	T <sub>3</sub> x <sup>4</sup>	3476.84	3.4	93.4	0	0.7	2.3	0.2	66	0	0	0	0	0	34
X11	T <sub>3</sub> x <sup>4</sup>	3478.90	7	91.9	0	0	0.8	0.3	58	0	0	0	0	16	26
X11	T <sub>3</sub> x <sup>4</sup>	3481.05	6	93.6	0	0	0.3	0.1	18	0	0	0	0	0	82
X11	T <sub>3</sub> x <sup>4</sup>	3481.66	16.1	83.4	0	0	0.3	0.2	55	0	0	0	0	0	45
X11	T <sub>3</sub> x <sup>4</sup>	3575.31	0	55.5	0	0	35.3	9.2	54	0	0	0	0	0	46
X11	T <sub>3</sub> x <sup>4</sup>	3579.55	0	61.6	0	0	26.3	12.1	73	0	0	0	0	0	27
CX568	T <sub>3</sub> x <sup>4</sup>	3402.10	6.8	89.3	0	0	1.8	2.1	63	0	0	0	0	22	15
CX568	T <sub>3</sub> x <sup>4</sup>	3403.45	1.5	96.7	0	0	1.3	0.5	39	0	0	0	0	50	11
CX568	T <sub>3</sub> x <sup>4</sup>	3404.10	7.3	90.6	0	0	1.4	0.7	31	10	0	0	0	39	20
CX568	T <sub>3</sub> x <sup>4</sup>	3405.03	6.4	90.3	0	0	1.7	1.6	44	0	0	0	0	40	16
CX568	T <sub>3</sub> x <sup>4</sup>	3406.22	9.7	88.6	0	0	0.9	0.8	22	20	0	0	0	43	15
CX568	T <sub>3</sub> x <sup>4</sup>	3406.77	7.1	89.6	0	0	2.4	0.9	37	5	0	0	0	39	19
CX568	T <sub>3</sub> x <sup>4</sup>	3408.59	5.1	92	0	0	2.2	0.7	28	18	0	0	0	35	19
CX568	T <sub>3</sub> x <sup>4</sup>	3410.71	6.5	92.5	0	0	0.6	0.4	53	0	0	0	0	25	22
CX568	T <sub>3</sub> x <sup>4</sup>	3412.35	2.2	96.8	0	0	0.5	0.5	51	0	0	0	0	37	12
CX568	T <sub>3</sub> x <sup>4</sup>	3414.23	5.9	93.1	0	0	0.6	0.4	52	0	0	0	0	36	12
CX568	T <sub>3</sub> x <sup>4</sup>	3422.85	6.1	90.1	0	0	3.5	0.3	39	0	0	0	0	30	31
CX568	T <sub>3</sub> x <sup>4</sup>	3424.87	5.1	93.3	0	0	0.8	0.8	53	0	0	0	0	27	20
CX568	T <sub>3</sub> x <sup>4</sup>	3426.10	7.3	90.8	0	0	1.5	0.4	36	0	0	0	0	16	48
CX568	T <sub>3</sub> x <sup>4</sup>	3428.36	2	67.5	0	0	19.3	11.2	53	0	0	0	0	0	47
CX568	T <sub>3</sub> x <sup>4</sup>	3469.00	5	79.7	0	0	11.9	3.4	43	0	0	0	0	32	25
CX568	T <sub>3</sub> x <sup>4</sup>	3481.10	6.8	43.2	0	0	26.5	23.5	22	0	0	0	0	72	6
CX568	T <sub>3</sub> x <sup>4</sup>	3546.66	10.2	84.9	0	0	2.8	2.1	26	0	0	0	0	57	17
CX568	T <sub>3</sub> x <sup>4</sup>	3713.17	7.5	80.5	0	0	9.7	2.3	27	0	0	0	0	58	15
CX568	T <sub>3</sub> x <sup>4</sup>	3714.05	4.6	83	0	0	10	2.4	31	0	0	0	0	54	15
CX568	T <sub>3</sub> x <sup>4</sup>	3715.00	3.8	90.7	0	0	4.5	1	17	6	0	0	0	55	22
CX568	T <sub>3</sub> x <sup>4</sup>	3721.37	0.20	47.5	0	0	40.3	12.2	41	8	0	0	0	30	21
<b>Average</b>			5.9	84.7	0	0	6.6	2.8	43	2.4	0	0	0	28.5	26.1

**Table 4** Electron probe characteristics of carbonate cement within the Xujiuhe sandstones of Xinchang structural belt

Stratigraphy	Type of cement	Oxide content (%)			molar fraction (%)			Samples
		MgO	CaO	FeO	MgCO <sub>3</sub>	CaCO <sub>3</sub>	FeCO <sub>3</sub>	
The second member	Dolomite cement	8.87	29.76	12.60	25.67	62.60	20.86	10
The second member	Calcite cement	0.67	53.26	1.49	1.67	95.73	2.09	5
The fourth member	Calcite cement	0.23	54.00	1.05	0.57	97.74	1.48	25
	Total	2.44	47.85	3.99	6.98	88.70	6.40	40

**Table 5.** Types and isotopic features of carbonate cements and fragments in the T<sub>3</sub>X<sup>4</sup> sandstone in Xinchang structural belt , Western Sichuan Basin.

Well	Depth (m)	Carbonate minerals	Types of occurrence	$\delta^{13}\text{C}_{\text{PDB}}$ (‰)	$\delta^{18}\text{O}_{\text{PDB}}$ (‰)
FG21	3516.74	Calcite cement	The primary pore	1.85	-10.06
CG561	3699.75	Calcite cement	The primary pore	0.24	-8.75
CF563	3744.21	Calcite cement	The primary pore	2.46	-5.51
FG21	3749.58	Calcite cement	The primary pore	1.07	-8.24
FG21	3764.75	Calcite cement	The primary pore	1.27	-6.86
FG21	3772.23	Calcite cement	The primary pore	2.15	-6.03
FG21	3776.7	Calcite cement	The primary pore	2.55	-4.75
CF563	3778.17	Calcite cement	The primary pore	2.31	-7.3
FG21	3778.7	Calcite cement	The primary pore	1.53	-6.41
FG23	3869.14	Calcite cement	The primary pore	-0.13	-9.92
XC22	3403.6	Calcite cement	The secondary pore	-2.85	-18.61
CX568	3404.1	Calcite cement	The secondary pore	-1.32	-13.61
CX568	3406.77	Calcite cement	The secondary pore	-1.2	-13.61
XC22	3412.08	Calcite cement	The secondary pore	-2.99	-17.89
CX568	3426.1	Calcite cement	The secondary pore	-0.76	-13.49
X11	3466.565	Calcite cement	The secondary pore	-3.47	-15.03
X11	3470.635	Calcite cement	The secondary pore	-2.93	-14.44
X11	3475.67	Calcite cement	The secondary pore	-3.61	-15.23
X11	3476.835	Calcite cement	The secondary pore	-2.31	-13.97
X11	3478.9	Calcite cement	The secondary pore	-3.19	-14.59
X11	3481.05	Calcite cement	The secondary pore	-2.44	-13.71
XC26	3481.81	Calcite cement	The secondary pore	-1.75	-17.4
XC26	3483.48	Calcite cement	The secondary pore	0.1	-10.77
XC26	3484.37	Calcite cement	The secondary pore	-0.08	-14.68
CF563	3511.77	Calcite cement	The secondary pore	-4.67	-19.71
CX560	3514.175	Calcite cement	The secondary pore	-1.46	-14.06
CX565	3547.62	Calcite cement	The secondary pore	-3.51	-15.29
CX565	3548.17	Calcite cement	The secondary pore	-2.99	-14.58
CX565	3549.33	Calcite cement	The secondary pore	-2.75	-14.65

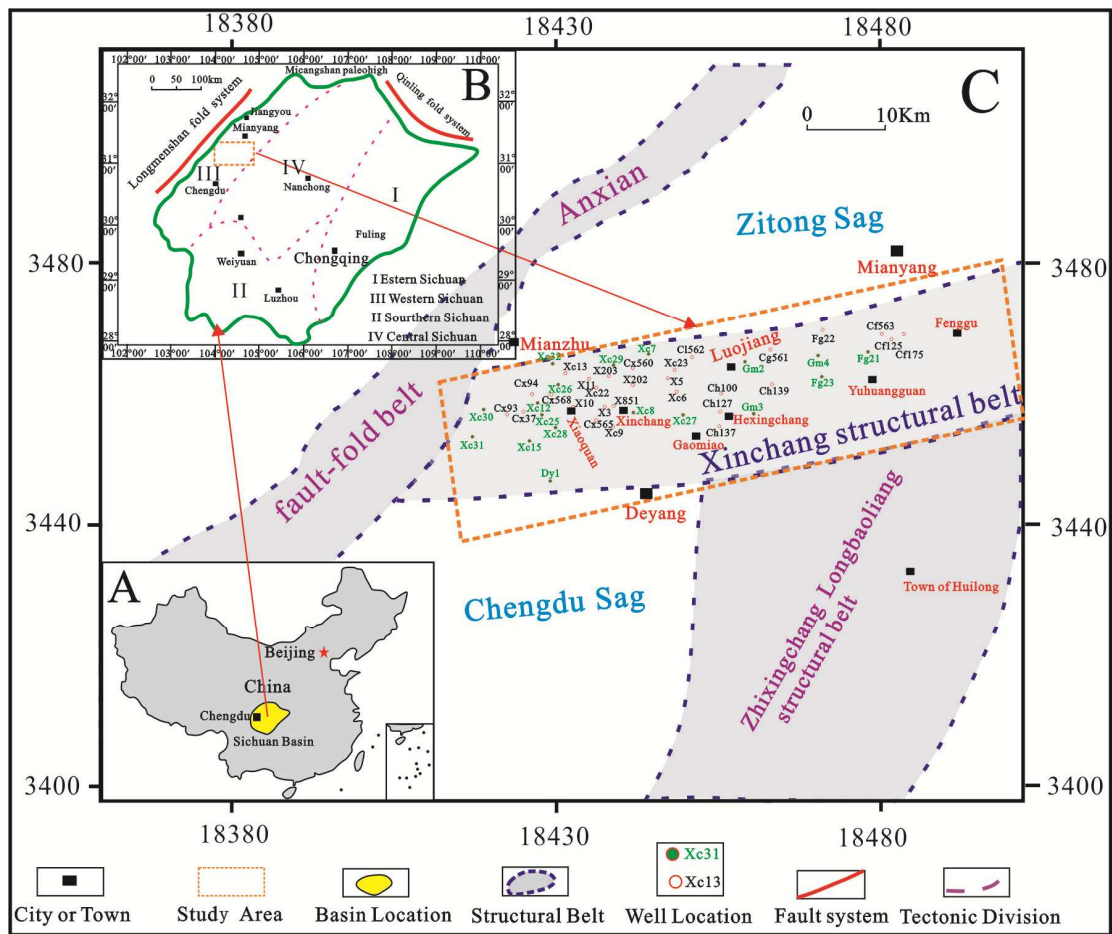
CX565	3558.33	Calcite cement	The secondary pore	-2.97	-14.59
XC29	3628.47	Calcite cement	The secondary pore	-3.37	-13.71
XC29	3629.75	Calcite cement	The secondary pore	-3.31	-12.87
CX565	3642.44	Calcite cement	The secondary pore	-5.43	-16.55
XC27	3661.82	Calcite cement	The secondary pore	-4.63	-14.99
XC27	3661.82	Calcite cement	The secondary pore	-3.42	-12.64
CG561	3694	Calcite cement	The secondary pore	-5.18	-18.93
CF563	3873.93	Calcite cement	The secondary pore	0.75	-15.42
CG561	4007.19	Calcite cement	The secondary pore	-1.92	-13.24
CX568	3469	Calcite	Rock fragment	1.92	-7.1
CX568	3721.37	carbonate	Rock fragment	1.35	-9.74
FG21	3767.45	carbonate	Rock fragment	1.63	-4.81
XC27	4018.12	carbonate	Rock fragment	1.85	-7.75
CX568	3410.71	Dolomite cement	The secondary pore	-0.97	-13.32
CX568	3414.23	Dolomite cement	The secondary pore	-0.81	-12.91
CF563	3873.93	Dolomite cement	The secondary pore	1.97	-10.94
XC28	3685.68	Domlomite	Rock fragment	1.33	-9.23
CF563	3744.21	Domlomite	Rock fragment	2.11	-5.64
FG21	3767.45	Domlomite	Rock fragment	2.01	-5.56
FG21	3775.6	Domlomite	Rock fragment	1.53	-5.99
FG21	3775.6	Domlomite	Rock fragment	2.22	-4.87
FG21	3776.7	Domlomite	Rock fragment	2.13	-5.45
CX568	3428.36	Domlomite	Rock fragment	1.46	-8.44
CX568	3481.1	Domlomite	Rock fragment	1.89	-7.8
CX568	3546.66	Domlomite	Rock fragment	1.72	-7.6
X11	3579.55	Domlomite	Rock fragment	1.5	-6.78

**Table 6.** Types and isotopic features of carbonate cements and fragments, in the T3x<sup>2</sup> sandstone in Xinchang structural belt, Western Sichuan Basin.

Well	Depth (m)	Carbonate minerals	Types of occurrence	$\delta^{13}\text{C}_{\text{PDB}}$ (‰)	$\delta^{18}\text{O}_{\text{PDB}}$ (‰)	Temp(°C)
XC12	4819.45	Calcite cement	The residual primary pore and secondary pore	-0.06	-16.65	117.5
GM2	4992.3	Calcite cement	The residual primary pore and secondary pore	-1.33	-16.09	113.3
GM4	5114.97	Calcite cement	The residual primary pore and secondary pore	0.05	-12.64	88.2
XC8	5175.37	Calcite cement	The residual primary pore and secondary pore	-0.11	-12.47	87.1
XC7	5287.98	Calcite cement	The residual primary pore and secondary pore	0.99	-12.98	90.6
XC7	5291.33	Calcite cement	The residual primary pore and secondary pore	1.15	-13.45	93.9
X11	4755.72	Calcite cement	The residual primary pore and secondary pore	0.05	-12.56	87.7
CG561	4997.72	Calcite cement	The residual primary pore and secondary pore	1.7	-16.36	115.3
X11	5070.01	Calcite cement	The residual primary pore and secondary pore	-1.25	-16.64	117.5
X11	5075.64	Calcite cement	The residual primary pore and secondary pore	-0.33	-10.88	76.4
GM2	4711.55	Dolomite cement	The secondary pore	0.53	-12	83.9
XC8	5009.28	Dolomite cement	The secondary pore	2.18	-12.17	85.0
GM2	5118.96	Dolomite cement	The secondary pore	3.69	-9.77	69.2
DY1	5323.87	Dolomite cement	The secondary pore	1.86	-15.17	106.4
X11	4757.765	Dolomite cement	The secondary pore	0.42	-9.97	70.5
X10	4851.34	Dolomite cement	The secondary pore	-0.38	-12.87	89.8
X10	4853.56	Dolomite cement	The secondary pore	2.5	-12.76	89.1
X10	4855.15	Dolomite cement	The secondary pore	1.68	-13.55	94.6
GM4	4889.09	Dolomite cement	The secondary pore	-1.81	-12.77	89.1
X10	4924.32	Dolomite cement	The secondary pore	4.97	-13.83	96.6
X10	4927.83	Dolomite cement	The secondary pore	8.7	-9.56	67.9
X10	4932.65	Dolomite cement	The secondary pore	-0.04	-14.36	100.4
X10	4937	Dolomite cement	The secondary pore	2.44	-11.94	83.5
X11	5022.52	Dolomite cement	The secondary pore	1.45	-10.3	72.6
CX565	5058.73	Dolomite cement	The secondary pore	0.4	-13.06	91.2
X11	5078	Dolomite cement	The secondary pore	-0.52	-14.47	101.2
DY1	5427.4	Dolomite cement	The secondary pore	2.58	-16.65	117.5
XC12	4812.34	Domlomite	Rock fragment	6.16	-8.79	
X10	4847.63	Domlomite	Rock fragment	1.25	-3.62	
CX565	5062.08	Domlomite	Rock fragment	1.01	-8.87	

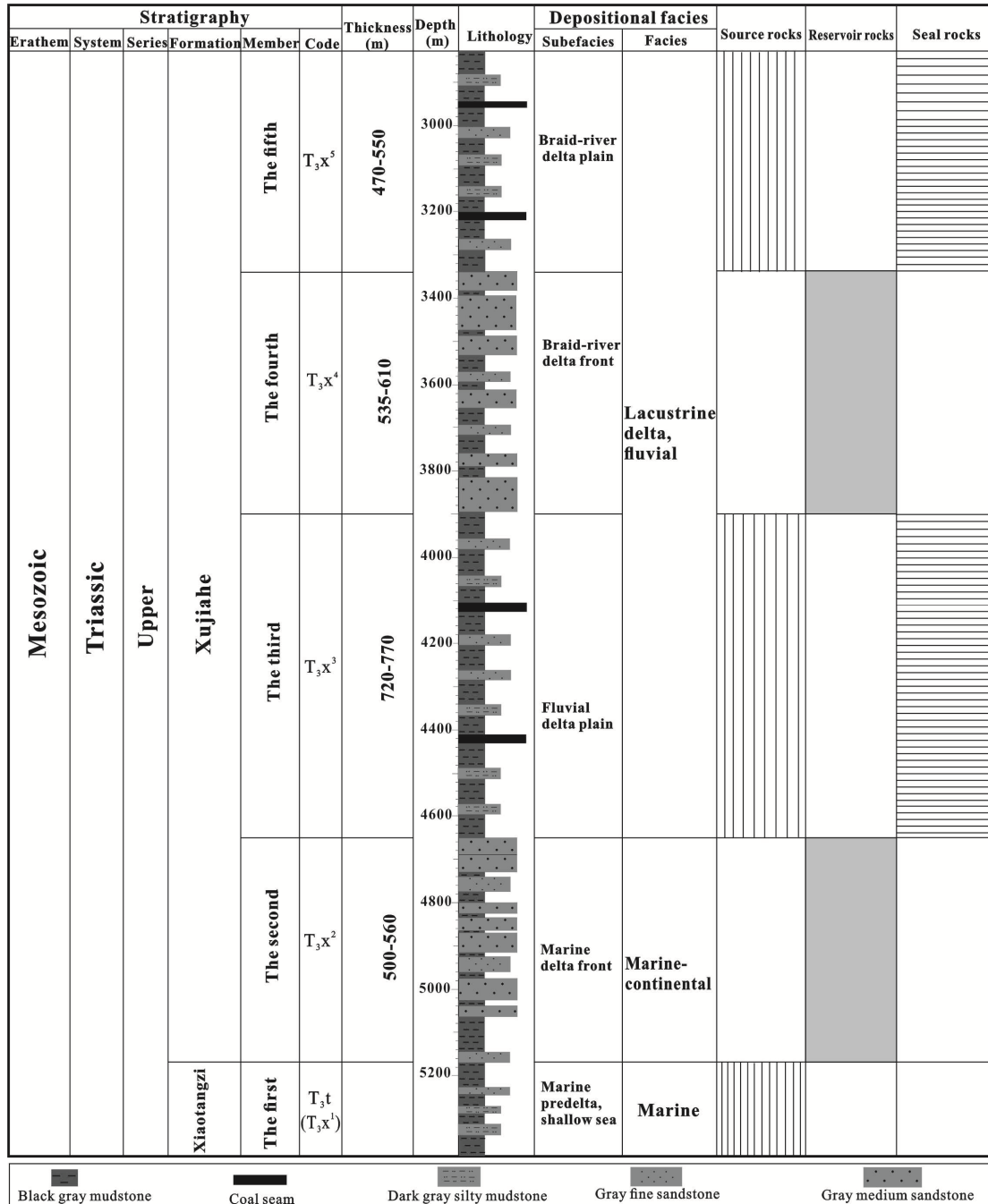
ACCEPTED MANUSCRIPT



1 **Figure captions**

2

3 Fig. 1. The geographical and structural map showing the location of the study area  
 4 which mainly comprises of the Xinchang structural belt. (A) Location map showing  
 5 the location of Sichuan basin in China. (B) The tectonic feature of Sichuan basin  
 6 indicates that the Western Sichuan basin foreland belong to the Western Sichuan  
 7 depression. (C) Structural map of the Western Sichuan foreland basin showing the  
 8 location of the Xinchang structural belt. Green wells represent key wells with  
 9 hydrocarbon show.



1

2

3

4

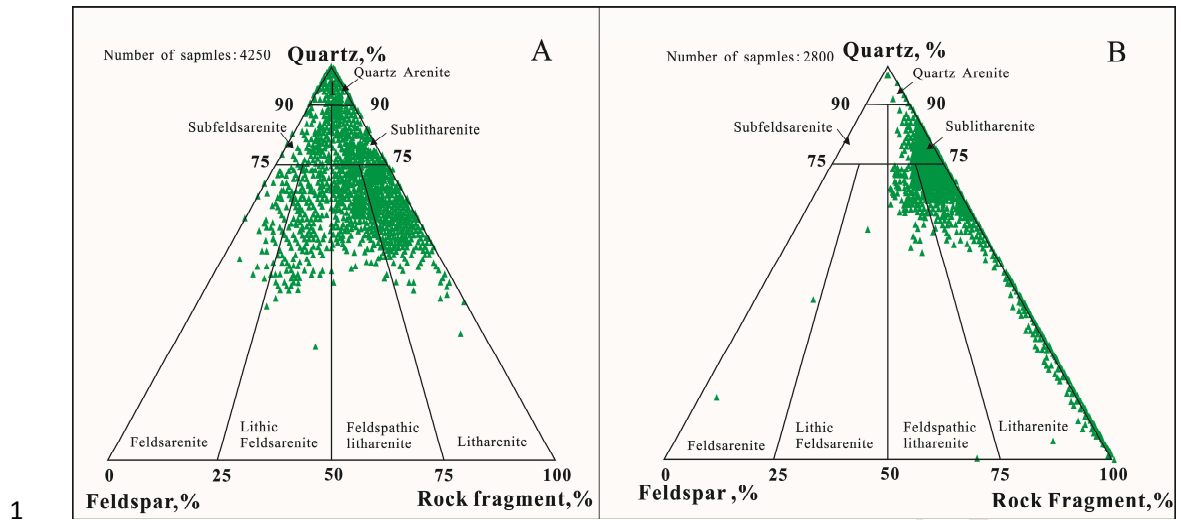
5

6

7

8

Fig. 2. Stratigraphic column of the Western Sichuan depression showing that the Xujiahe Formation sandstones. Abbreviations:  $T_3X^2$  = The second member of the Xujiahe Formation;  $T_3X^3$  = The third member of the Xujiahe Formation;  $T_3X^4$  = The fourth member of the Xujiahe Formation;  $T_3X^5$  = The fifth member of the Xujiahe Formation.  $T_3X^1$  = The Xiaotangzi and Maantang Formations,

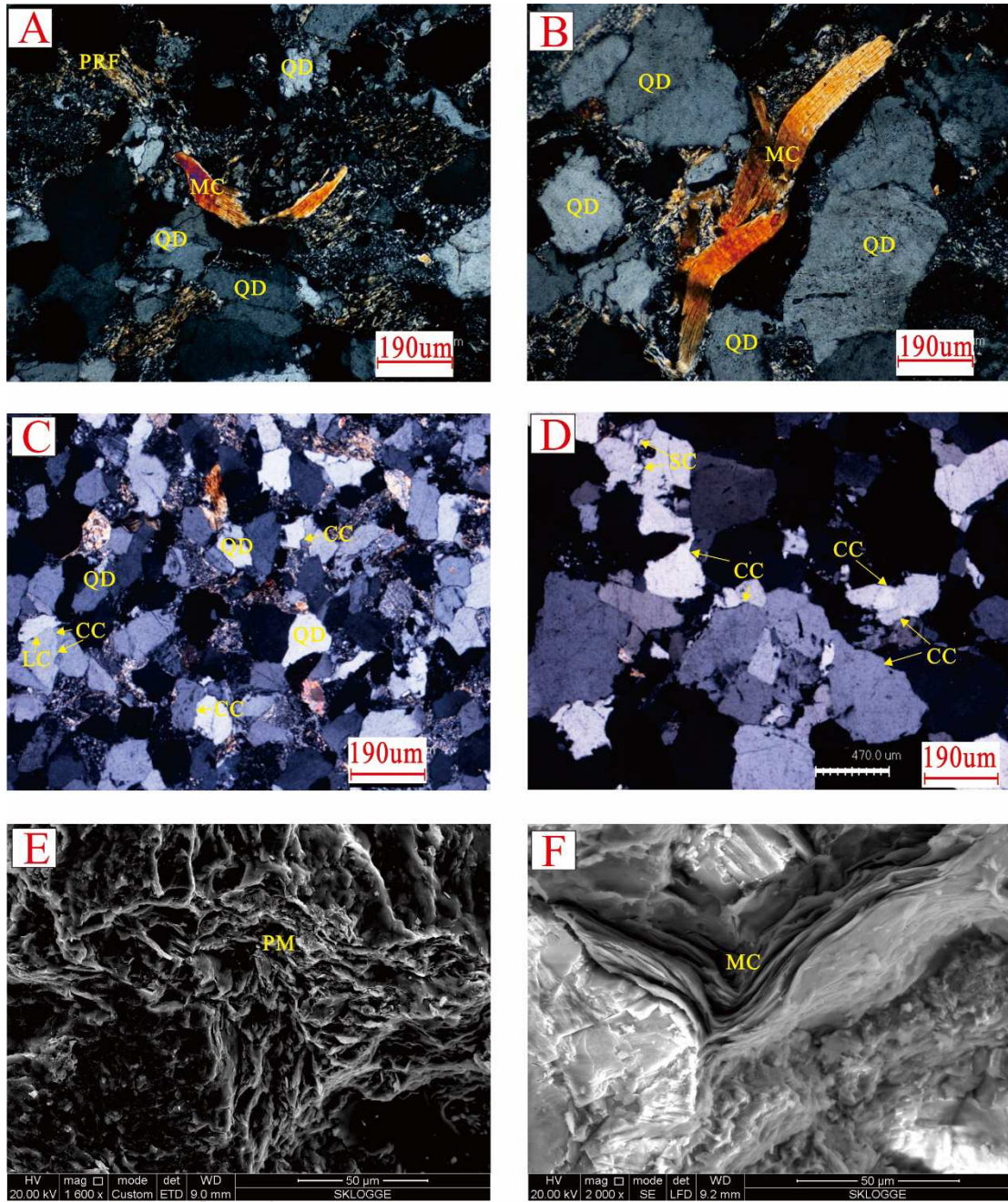


1

2 Fig. 3. Ternary plots showing grain composition of sandstones from  $T_3x^2$  sandstone (A)3 and  $T_3x^4$  sandstone (B) (refer to sandstone classification standard of Folk et al.,

4 1980)

5



1  
 2 Fig. 4. The compaction characteristics in the  $T_3x^2$  and  $T_3x^4$  sandstones.(A) Optical  
 3 photomicrographs of thin section (XPL) showing the deformation of mica (MC) and  
 4 plastic rock fragments (PRF), pseudomatrix from mud intraclasts. Well XC27,  
 5 3589.91m,  $T_3x^4$ . (B) Optical photomicrographs of thin section (XPL) showing the  
 6 deformation of mica (MC).well DY1,4197.63m,  $T_3x^4$ .(C) Optical photomicrographs  
 7 of thin section (XPL) showing the long (LC) and concave-convex contacts(CC)  
 8 between quartz-quartz grains. Well XC15, 4950.7m,  $T_3x^2$ . (D) Optical

1 photomicrographs of thin section (XPL) showing the concave–convex (CC) and  
2 sutured contacts (SC) between quartz–quartz grain. well XC12, 4828.44m, T<sub>3</sub>x<sup>2</sup>. (E)  
3 SEM image showing the pseudomatrix formed by the deformation of plastic rock  
4 fragments. well DY1,5320.05m, T<sub>3</sub>x<sup>2</sup>.(F) SEM image showing the deformation of  
5 mica (MC).well XC31,3741.77m, T<sub>3</sub>x<sup>4</sup>.

6

7

8

9

10

11

12

13

14

15

16

17

18

19

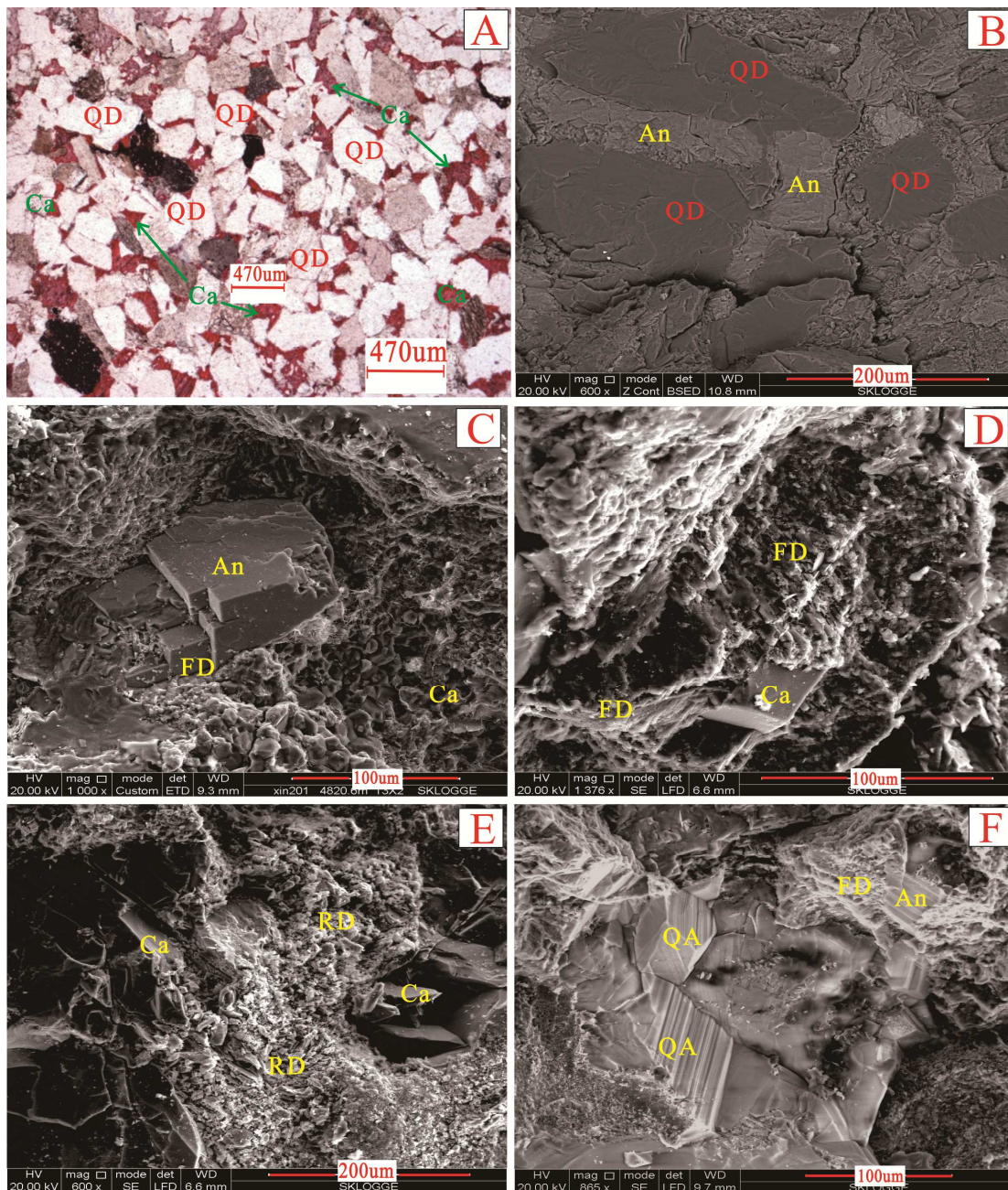
20

21

22

23

24



1  
2 Fig. 5. The carbonate cement characteristics in the  $T_3x^2$ : (A) Optical photomicrograph  
3 (PPL) showing the calcite (Ca) filling in the intergranular pores, QD-detriral quartz,  
4 Well GM2,4722.33m, $T_3x^2$  (B) BSE image showing dolomite (ankerite) cement (An)  
5 filling the intergranular pores, well GM2, 4822.0m,  $T_3x^2$ . (C) SEM image showing  
6 the euhedral dolomite(ankerite) (An) filling the intragranular dissolved pores, well  
7 X201, 4820.6m,  $T_3x^2$ . (D) SEM image showing calcite(Ca) replacing the feldspar  
8 with the dissolution(FD),well GM4,4887.85m,  $T_3x^2$ .(E) SEM image showing calcite

1 replacing the rock fragments accompanying with the dissolution(RD), GM4,4887.85m,  
2  $T_3x^2$ .(F) SEM image showing authigenic dolomite(ankerite) (An) and quartz(QA)  
3 replacing feldspar and filling the dissolved pore of feldspar, which suggest calcite  
4 and quartz cement are related with the feldspar dissolution(FD). well  
5 GM3,4922.21m,  $T_3x^2$ .

6

7

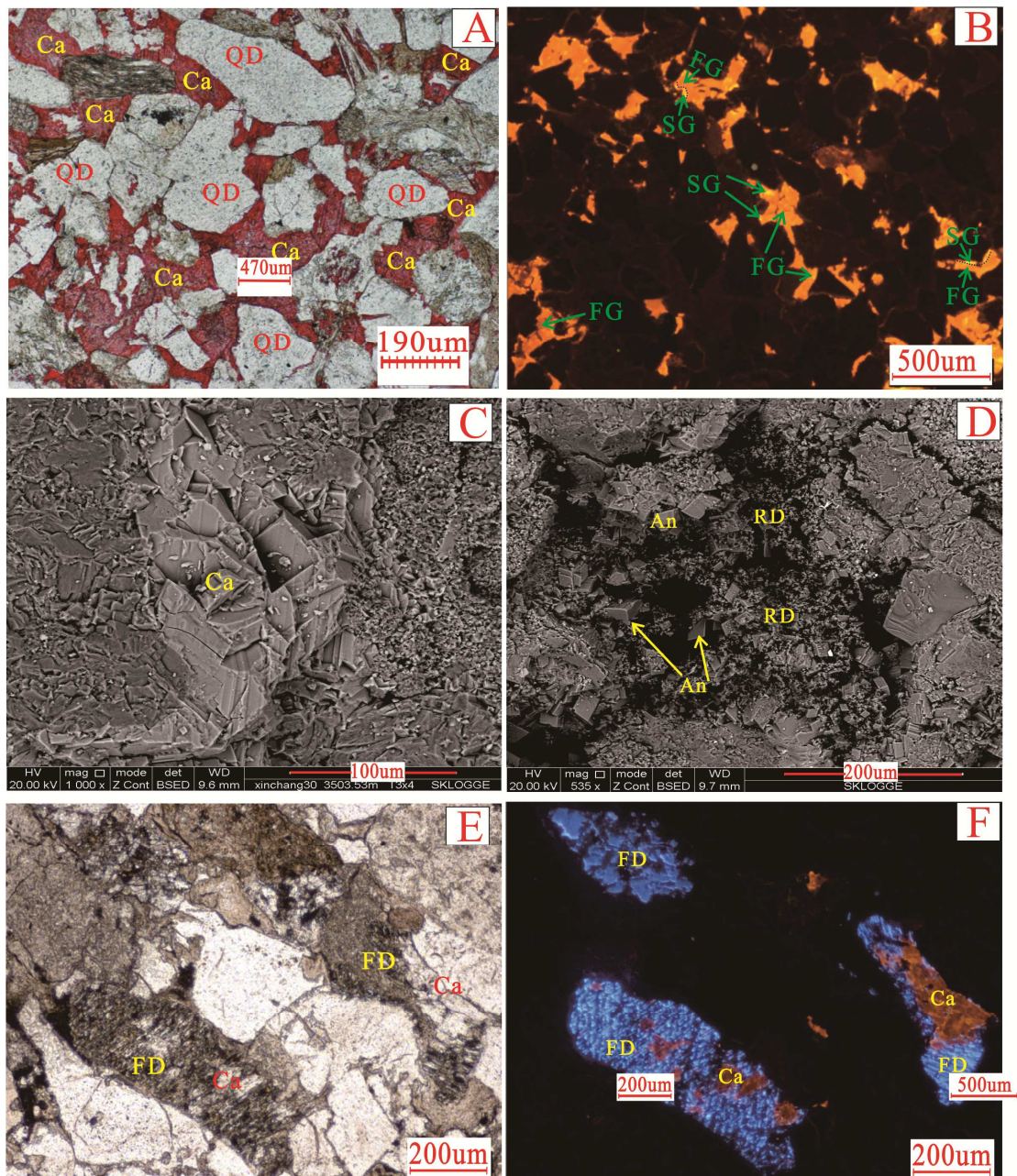
8

9

10

11

12



1

2 Fig. 6. The carbonate cement characteristics in the  $T_3x^4$  sandstones: (A) Optical  
 3 photomicrograph (PPL) showing basal calcite cement (Ca) filling the intergranular  
 4 pores, well XC15, 3636.57m,  $T_3x^4$ . (B) Cathodoluminescence image showing two  
 5 generation of calcite: saffron yellow micro-crystal calcites filling the primary pores  
 6 represent the first generation (FG), the orange red calcite cements filling residual  
 7 primary pore and secondary pores as partially replacement of some detrital grains,  
 8 represent the second generation (SG).well X5, 3673.43m,  $T_3x^4$ . (C) BSE image



1 showing calcite (Ca) filling in the intergranular pores, well XC30,3503.53m,  $T_3x^4$ .  
2 (D) BSE image showing authigenic euhedral dolomite (ankerite) (An) filling in the  
3 intergranular dissolved pores that formed by dissolution of carbonate rock fragments,  
4 well FG21, 3758.6m,  $T_3x^4$ .(E) Optical photomicrograph (PPL) showing calcite(Ca)  
5 replacing the feldspar with the dissolution(FD), well X5,3598.59m, $T_3x^4$ .(F).  
6 Cathodoluminoscope image responding to the (E) shows the saffron yellow calcite  
7 cements (Ca) replacing the blue feldspar, and the intragranular dissolved pores  
8 caused by the feldspar dissolution (FD). well X5,3598.59m, $T_3x^4$ .

9

10

11

12

13

14

15

16

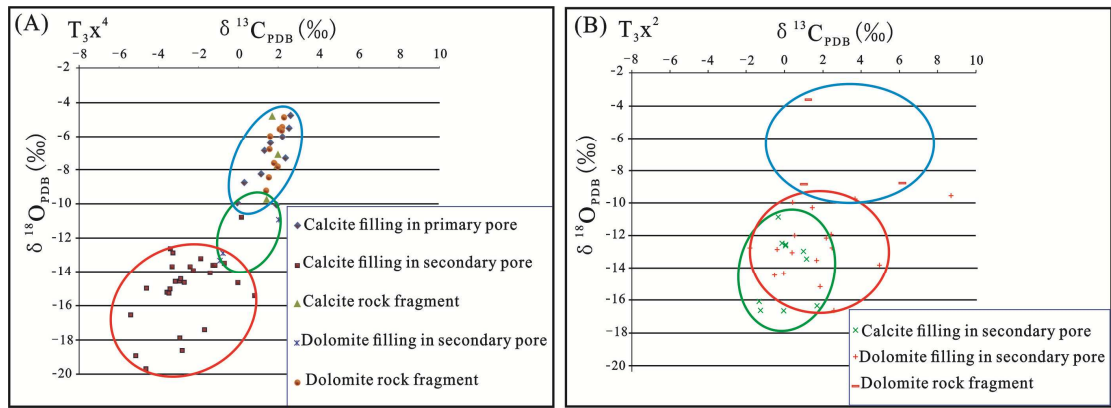
17

18

19

20

21



1

2 Fig. 7. The  $\delta^{18}\text{O}$ - $\delta^{13}\text{C}$  diagram of various carbonate cement within the sandstones of  
 3 the  $\text{T}_3\text{X}^4$  (A) and  $\text{T}_3\text{X}^2$  (B) of the Xujiahe Formation.

4

5

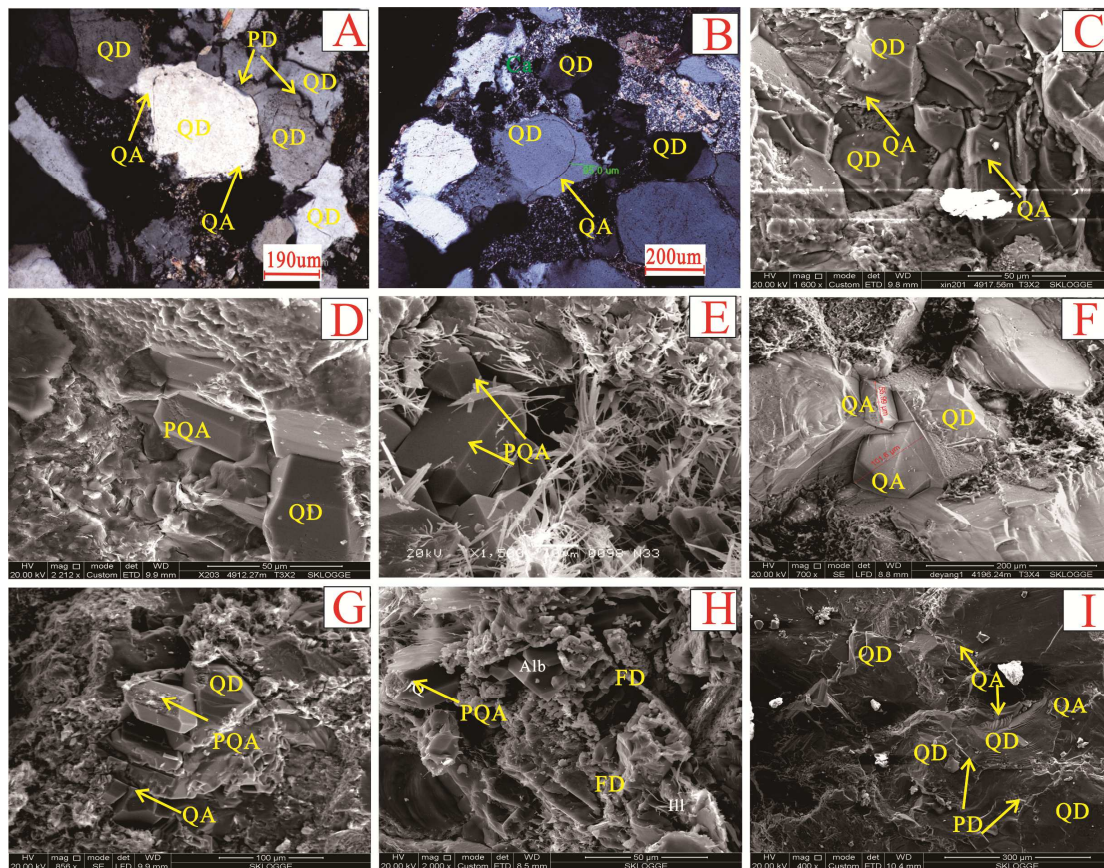
6

7

8

9

10



1  
 2 Fig. 8. The quartz cement characteristics in the  $T_3x^2$  and  $T_3x^4$  sandstones.(A) The  
 3 optical photomicrograph of thin section (PPL) showing quartz  
 4 overgrowth(QA),which occur near the pressure dissolution(PD),QD- detrital quartz.  
 5 well DY1,5341m,  $T_3x^2$  . (B) The optical photomicrograph of thin section (PPL)  
 6 showing quartz overgrowth (QA), QD-detrital quartz. well XC25,3775.25m,  $T_3x^4$  . (C)  
 7 SEM image showing quartz overgrowth (QA), QD- detrital quartz. Well  
 8 X201,4917m,  $T_3x^2$ .(D) SEM image showing isolated pore-filling authigenic quartz  
 9 crystal (PQA),,well X203,4912.27m,  $T_3x^2$ .(E) SEM image showing the isolated  
 10 authigenic quartz crystals (PQA) and illite(I) filling the intergranular pores,well  
 11 CX568,3412.35m,  $T_3x^4$  . (F) SEM image showing the quartz overgrowth(QA),well  
 12 DY1,4196.24m,  $T_3x^4$ .(G) SEM image showing the authigenic quartz including the  
 13 isolated pore-filling quartz crystal(PQA) and quartz overgrowth(QA), both of which  
 14 were partly replaced by the illite(I).well GM3,3780.2m  $T_3x^4$ .(H) SEM image

1 showing the isolated pore-filling authigenic quartz (PQA), albite (Alb) and illite (I)  
2 filling in the dissolved pores which were formed by the feldspar dissolution (FD).

3 Well X201, 4917.0m, T<sub>3x</sub><sup>2</sup>. (I) SEM image showing the quartz overgrowth (QA) occur  
4 together with the pressure dissolution (PD). well GM2, 4736m, T<sub>3x</sub><sup>2</sup>.

5

6

7

8

9

10

11

12

13

14

15

16

17

18

19

20

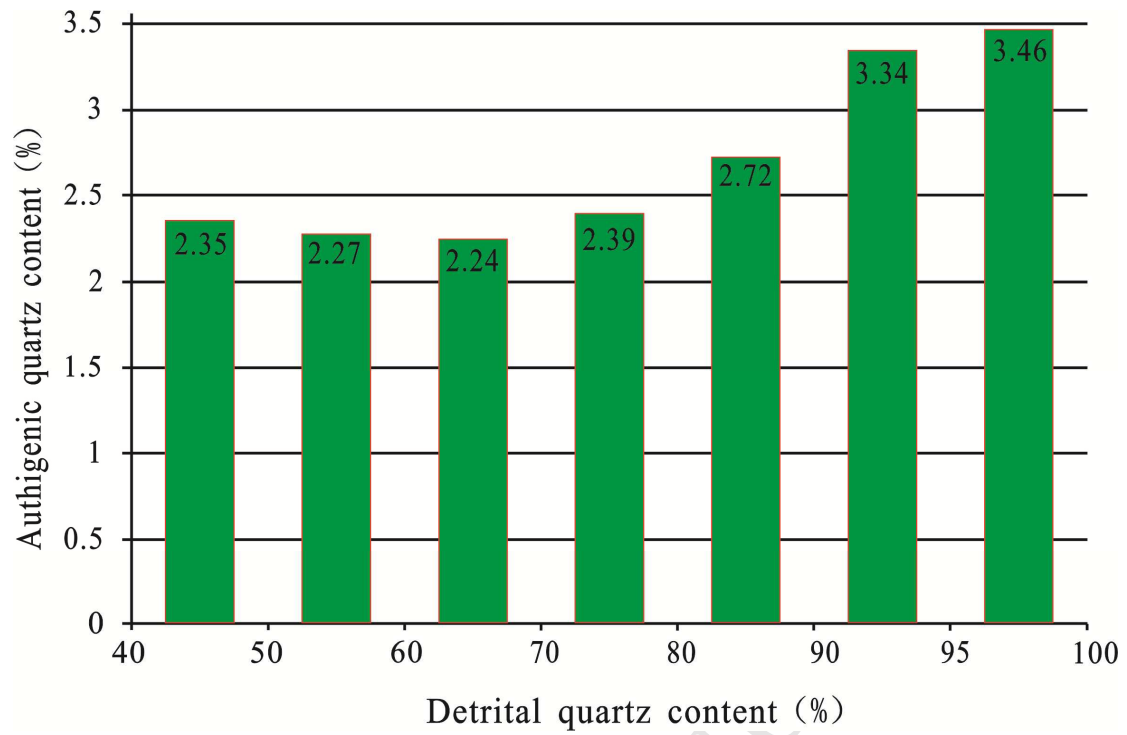
21

22

23

24

25



1

2 Fig. 9. The average content relationship between the detrital quartz and the authigenic  
3 quartz cements.

4

5

6

7

8

9

10

11

12

13

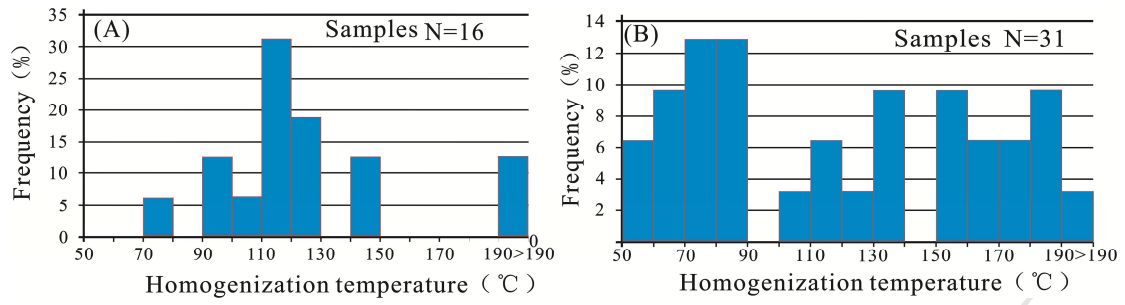
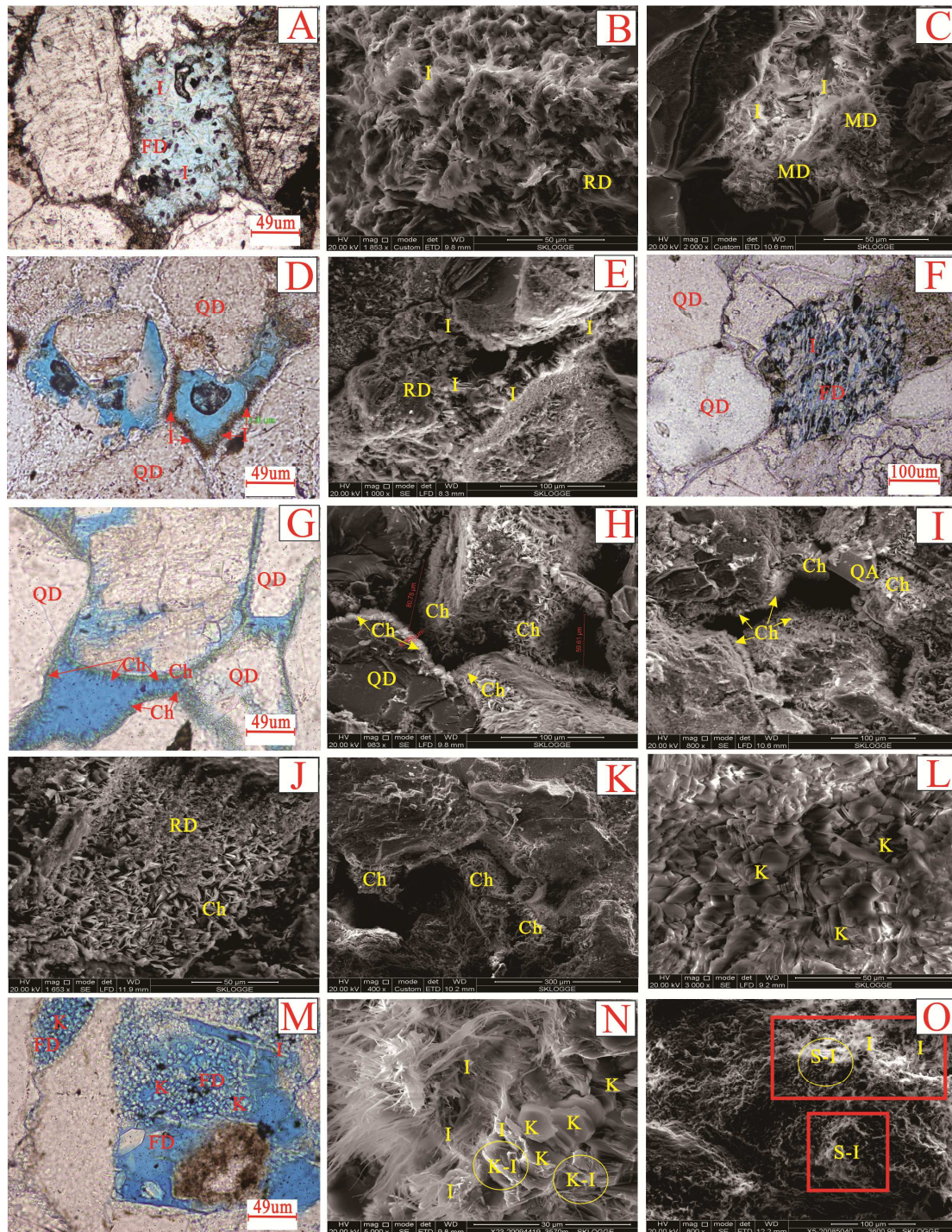


Fig. 10. Frequency histogram of homogenization temperature from inclusions in authigenic quartz cements in the  $T_3x^4$  (A) and  $T_3x^2$  (B) (Luo et al., 2015).

1  
2  
3  
4  
5  
6  
7  
8  
9  
10  
11  
12  
13  
14



1

2 Fig. 11. The clay minerals characteristics in the  $T_3x^2$  and  $T_3x^4$  sandstones.(A) The  
 3 optical photomicrograph of thin section (PPL) showing authigenic illite (I) occurring  
 4 as netted aggregates filled in intragranular dissolved pores., which is related with the  
 5 feldspar dissolution(FD). well X10,4884.53m,  $T_3x^2$ .(B) SEM image showing illite(I)  
 6 replaced the rock fragments,which is related with rock fragments

1 dissolution(RD).well GM2,4714.69m,  $T_3x^2$ . (C) SEM image showing non-netted  
2 aggregates illite related with the illitization of matix. well GM2,4714.69m,  $T_3x^2$ . (D)  
3 The optical photomicrograph of thin section (PPL) showing authigenic illite(I)  
4 occurring as grain-coatings. well XC27,3670.64m,  $T_3x^4$ .(E) SEM image showing the  
5 filamentous(netted aggregates) illite filling in the dissolved pore of rock  
6 fragments.3787.4m.  $T_3x^4$ . (F) The optical photomicrograph (PPL) showing  
7 authigenic illite occurring as netted aggregates filled in intragranular dissolved pores  
8 of feldspar.well X5,3673.47m,  $T_3x^4$ .(G) The optical photomicrograph (PPL) showing  
9 the the chlorite rim(Ch) occurring as grain-coating. well CG561,4992.9m,  $T_3x^2$ .(H)  
10 SEM image showing the chlorite rim(Ch) as the grain-coating.well DY1,5530.86m,  
11  $T_3x^2$ . (I)SEM image showing the chlorite rim(Ch) as the grain-coating accompanied  
12 by authigenetic quartz (QA) filling intergranular pores well GM2,5038.9m,  $T_3x^2$ . (J)  
13 SEM image showing chlorite (Ch) filling in the dissolved pore formed by the rock  
14 volcanic fragments dissolution (RD).well GM2,4994.06m,  $T_3x^2$  . (K) SEM image  
15 showing the pore-filling chlorite. well GM4, 3786.11m,  $T_3x^2$ . (L) SEM image  
16 showing pseudo-hexagonal kaolinite occurring as vermicular or booklet-like  
17 aggregates. well FG21,3755.49m,  $T_3x^4$ .(M) The optical photomicrograph (PPL)  
18 showing kaolinite(K) formed by the feldspar dissolution(FD). Well  
19 CX565,3549.53m,  $T_3x^4$ .(N) SEM image showing booklet-like pseudo-hexagonal  
20 kaolinite(K) which partly transformed into the filamentous illite(I).well  
21 XC23,3570m,  $T_3x^4$ .(O) SEM image shows the flaky smectite transforming into  
22 filamentous illite(I) ,(S-I)-mixed layer I/S. well X5,3600.99m,  $T_3x^4$ .

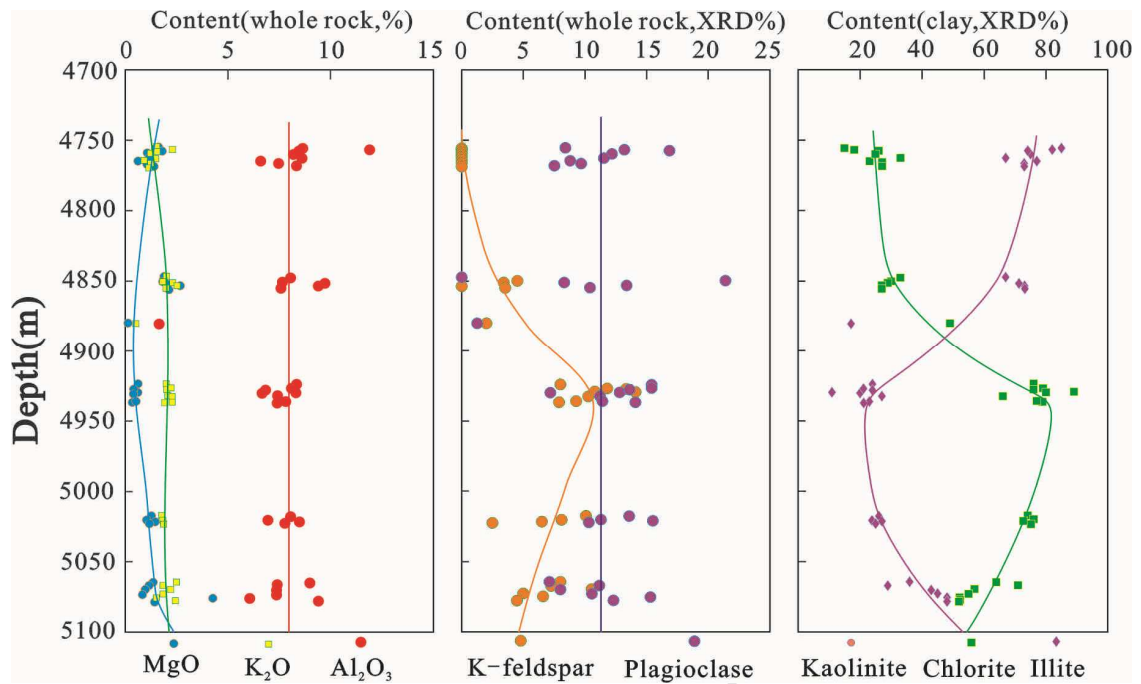
23

24

25



1



2

3 Fig. 12. Vertical variation of the content of typical major elements, feldspar and clay  
 4 minerals in the  $T_3x^2$  sandstones. The content of kaolinite, chlorite and illite represent  
 5 relative content in clay minerals.

6

7

8

9

10

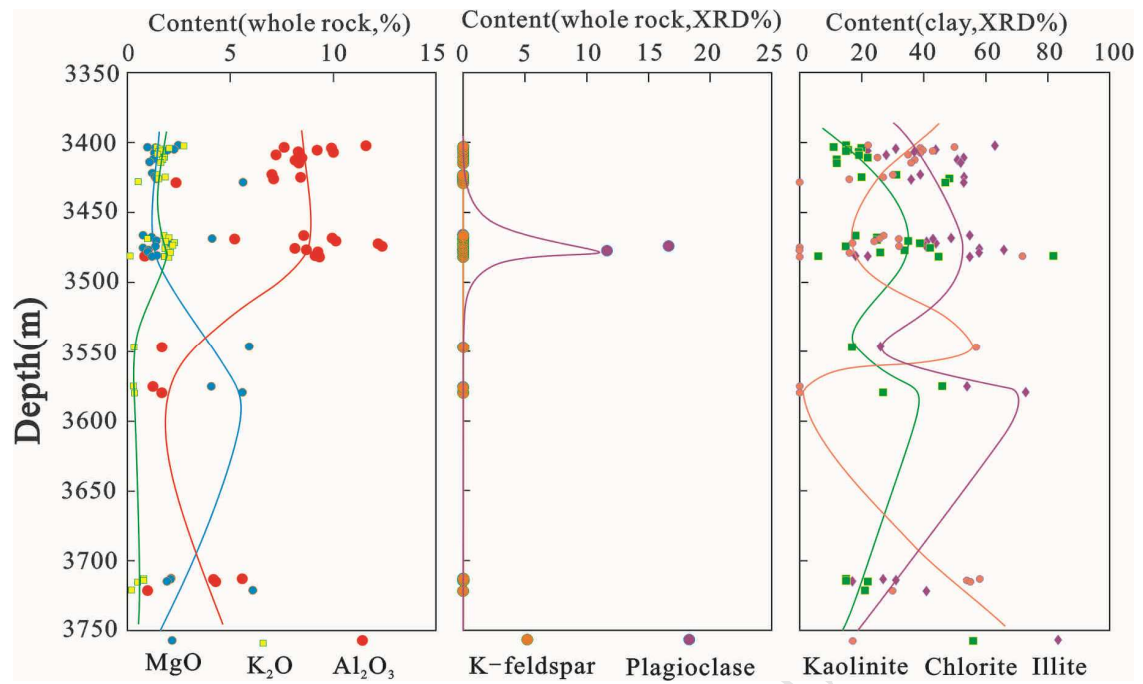
11

12

13

14

15



1

2

Fig. 13. Vertical variation of the content of typical major elements, feldspar and clay minerals in the  $T_3x^4$  sandstones. The content of kaolinite, chlorite and illite represent relative content in clay minerals.

3

4

5

6

7

8

9

10

11

12

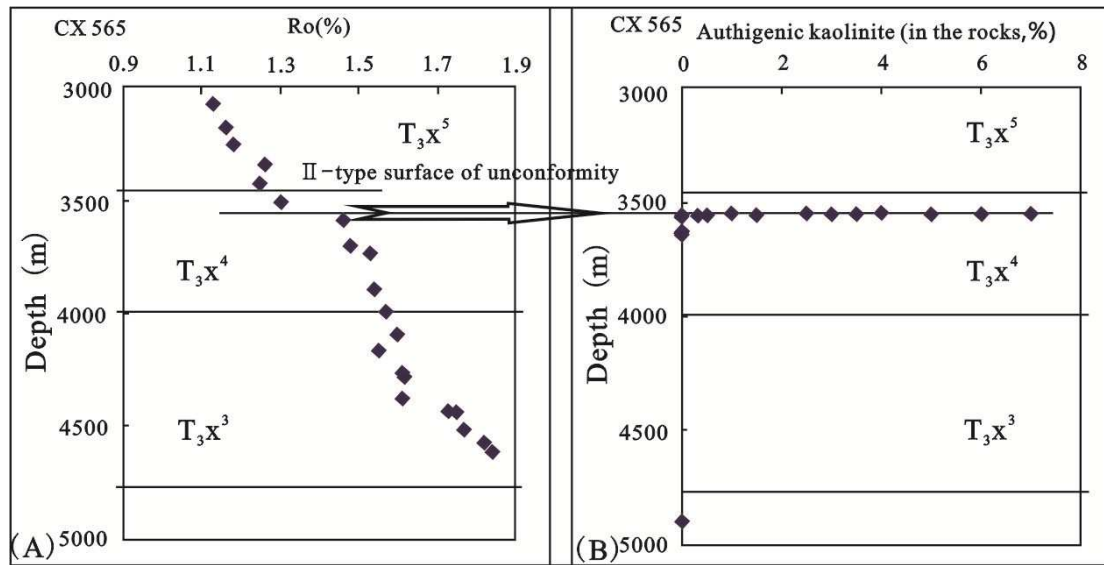
13

14

15

16

17



1

2 Fig. 14. The scatter diagram of Ro –depth and kaolinite-depth in the Xujiahe

3 Formation of well CX565 (Based on Zhang, 2011). (a) The Ro –depth scatter

4 diagram of the well CX565 show an outlier of the Ro exist in the top of the  $T_3X^4$ . (a)

5 and (b) indicate that the depth of outlier of Ro corresponds to the developmental

6 zone of kaolinite.

7

8

9

10

11

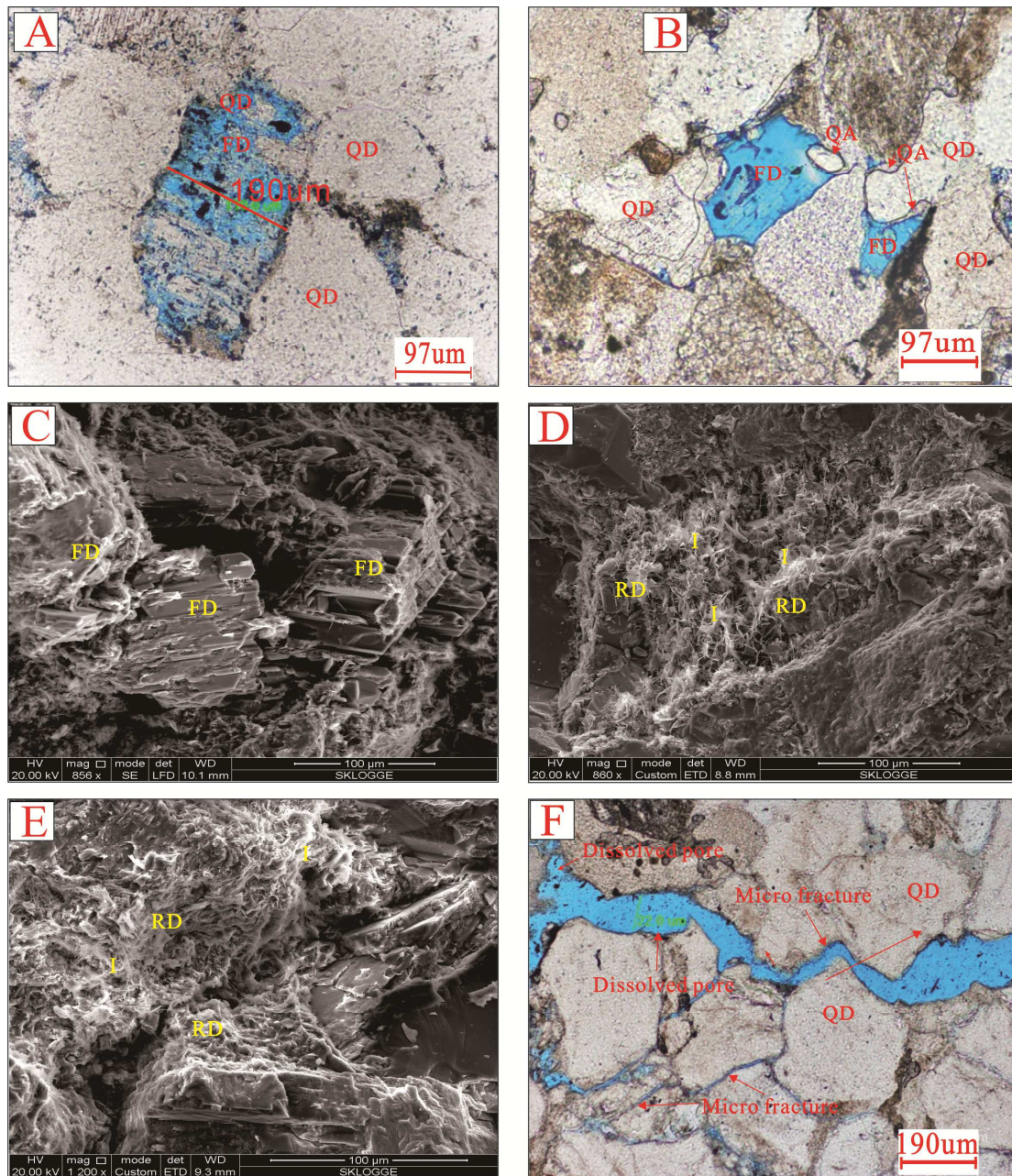
12

13

14

15

16



1  
 2 Fig. 15. The dissolution characteristics of feldspar and rock fragments in the T3X2  
 3 and T<sub>3</sub>X<sup>4</sup> sandstones. (A) Optical photomicrographs of thin section(PPL) showing  
 4 the feldspar partly dissolved.well GM4,3788.92m, T<sub>3</sub>X<sup>4</sup>.(B) Optical  
 5 photomicrographs of thin section(PPL) showing the feldspar completely  
 6 dissolved.well xc15,3625.28m, T<sub>3</sub>X<sup>4</sup>.(C) SEM image showing feldspar partly  
 7 dissolved. well GM3,4079.48m, T<sub>3</sub>X<sup>4</sup>.(D) SEM image showing the illite (I)  
 8 accompanying the rock fragment dissolution (FD).well GM4,4888.77m, T<sub>3</sub>X<sup>2</sup>.(E )

1 SEM image showing the illite (I) accompanying the rock fragment dissolution  
2 (FD).well gm4,4087.11m, T<sub>3</sub>x<sup>4</sup>.(F) Optical photomicrographs of thin section(PPL)  
3 showing the dissolved pore related with the enlarged dissolution of the  
4 micro-fractures.wellXC15,3962.66m, T<sub>3</sub>x<sup>4</sup>.

5

6

7

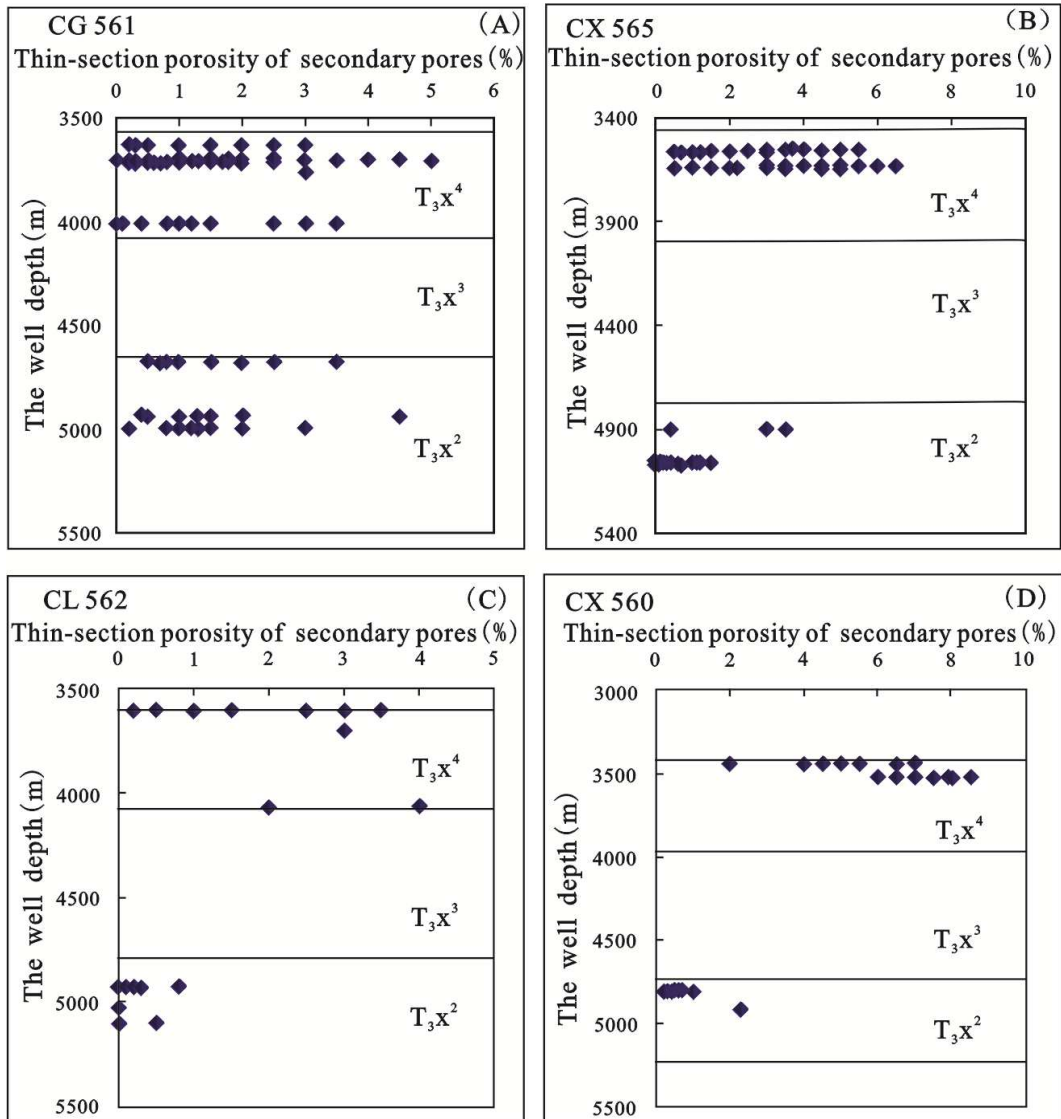
8

9

10

11

12



1  
2 Fig. 16. Distribution characteristic of the secondary pores within the Xujiache  
3 Formation sandstones reservoir of study area (Zhang, 2011). (A) ,(B) ,(C) and (D)  
4 show that most of secondary pores usually occurred in the top of the  $T_3X^4$ , and some  
5 others in the bottom of the  $T_3X^4$  and the middle-upper part of  $T_3X^2$ .

6

7

8

9

10

11

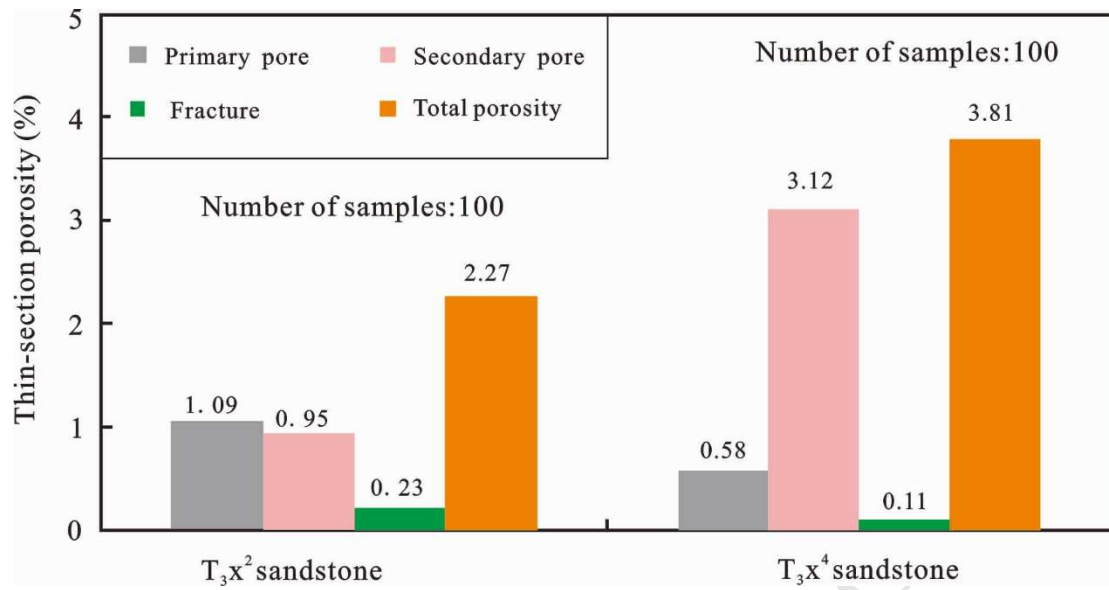


Fig. 17. Thin-section porosity of different types of pore in the  $T_3x^2$  and  $T_3x^4$  sandstone.

1  
2  
3  
4  
5  
6  
7  
8  
9  
10  
11  
12  
13  
14  
15  
16  
17

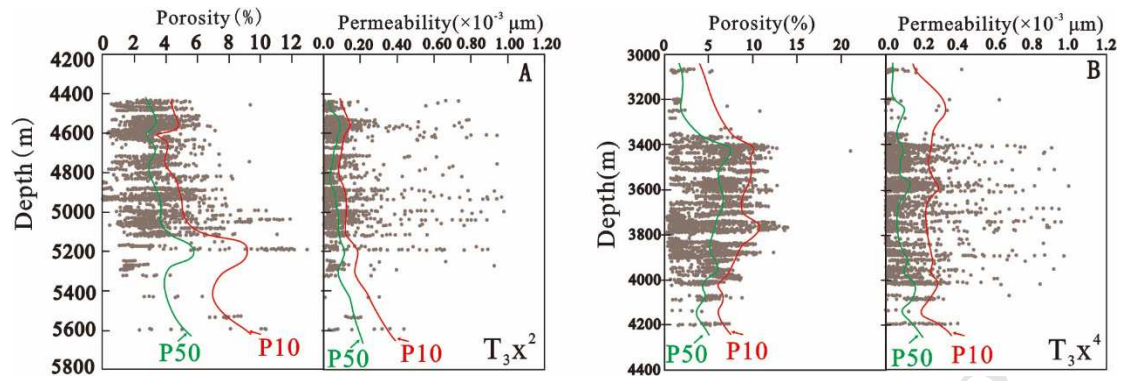
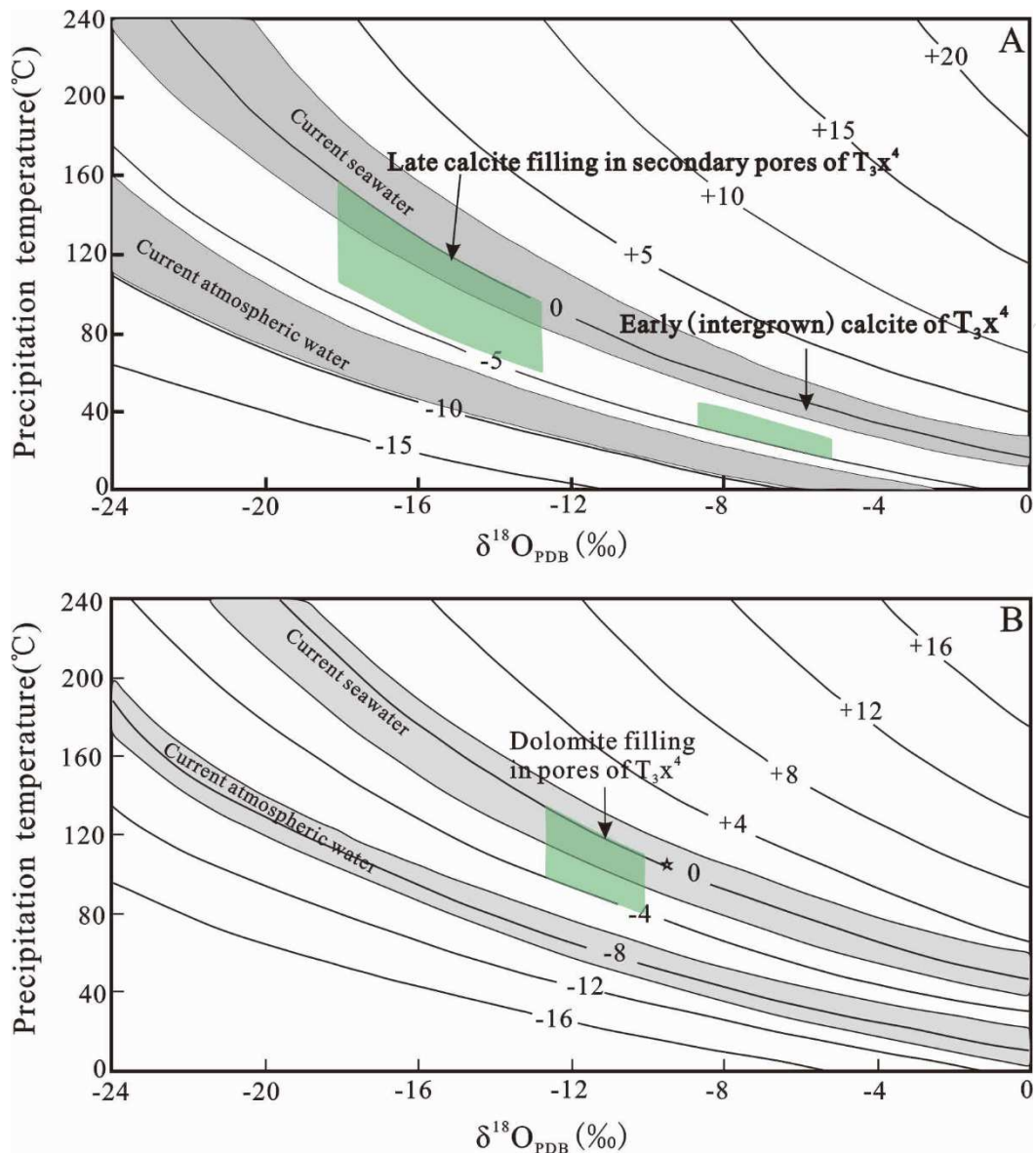
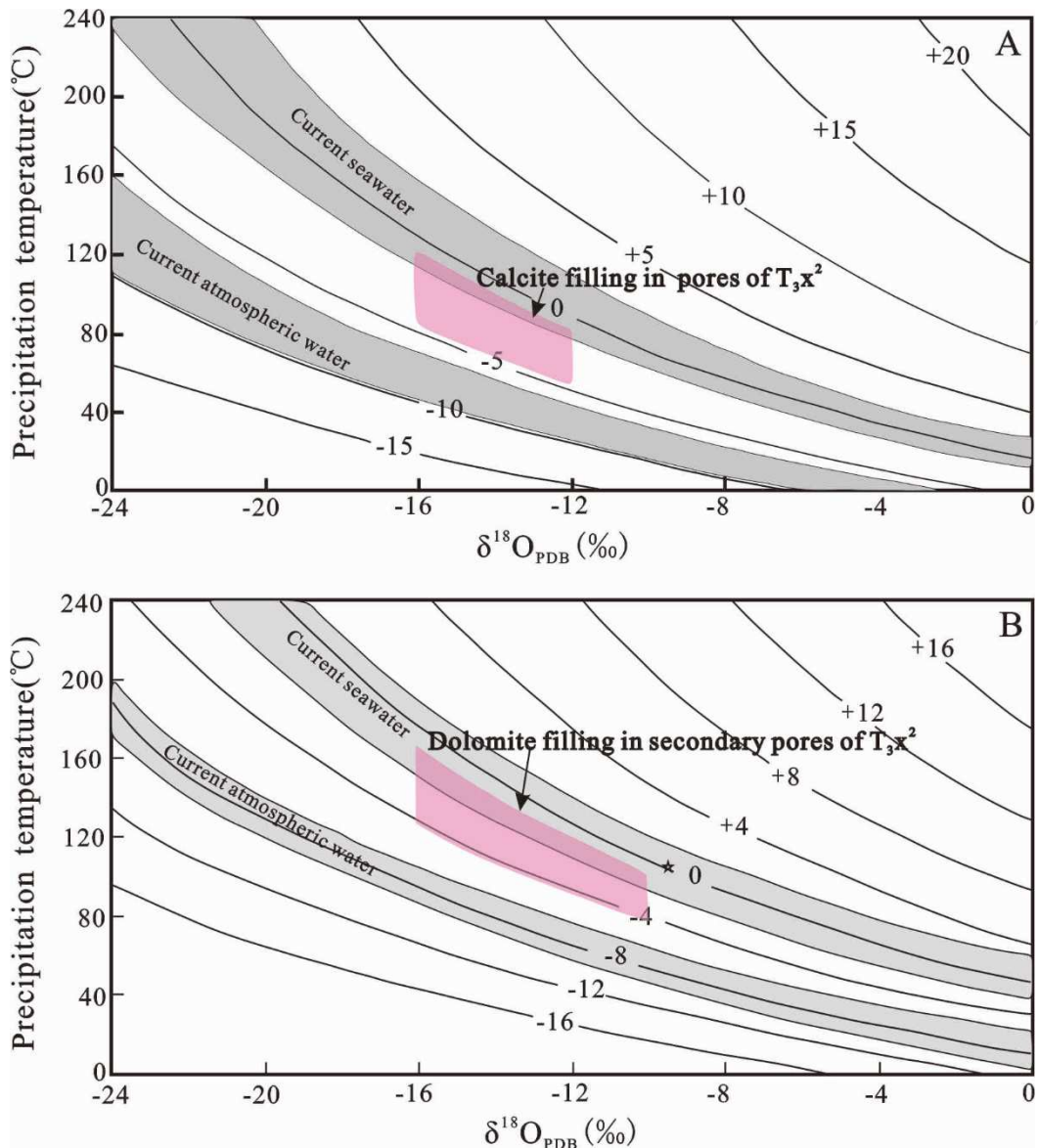


Fig. 18. Core porosity versus depth and core permeability versus depth profiles of the  $T_3x^2$  sandstones (A) and  $T_3x^4$  sandstones (B) in the Xinchang structural belt. Porosity values and permeability values of P10 (10% of reservoir has porosity greater than this value), P50(median) values were calculated for each 0.2-km(0.124-mi)depth interval from starting depth of 4.2km( $T_3x^2$ ) and 3.0km( $T_3x^4$ ) respectively.

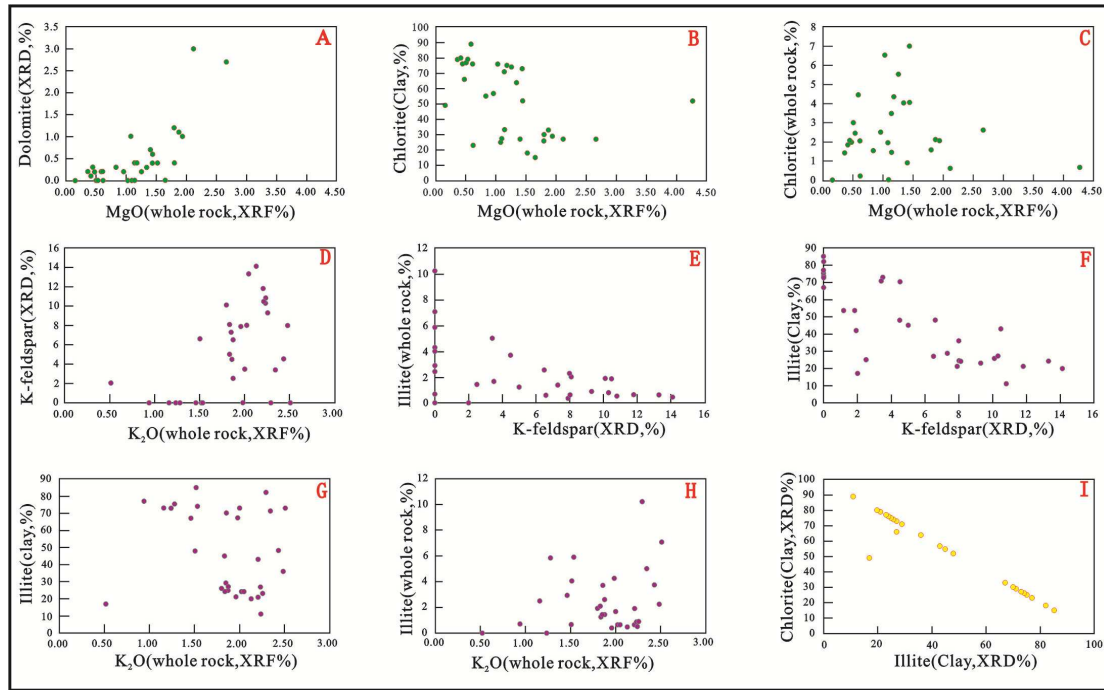




1  
 2 Fig. 19. Cross plot of  $\delta^{18}\text{O}_{\text{PDB}}$  values of the authigenic calcite (A) and dolomite  
 3 cements(B) within the  $\text{T}_3\text{x}^4$  sandstones in the Xinchang structural belt in equilibrium  
 4 with water  $\delta^{18}\text{O}_{(\text{SMOW})}$  values (-15‰, -10‰, -5‰, 0‰, +5‰, +10‰, +15‰, +20‰)  
 5 as a function of precipitation temperature (Friedman and O'Neil, 1977). The contours  
 6 (SMOW) represent oxygen isotopic composition of carbonate balanced fluids. The  
 7  $\delta^{18}\text{O}_{\text{water (SMOW)}}$  values of carbonate balanced fluids within the  $\text{T}_3\text{x}^4$  sandstones  
 8 originate from the Liu et al., 2014a,b and Shen et al.,2010.The green shapes were  
 9 bounded by the authigenic carbonate cements and the  $\delta^{18}\text{O}_{\text{water (SMOW)}}$  values of  
 10 carbonate balanced fluids.



1  
 2 Fig. 20. Cross plot of  $\delta^{18}\text{O}_{\text{PDB}}$  values of the authigenic calcite (A) and dolomite  
 3 cements(B) within the  $T_3x^2$  sandstones in the Xinchang structural belt in equilibrium  
 4 with water  $\delta^{18}\text{O}_{(\text{SMOW})}$  values (-15‰, -10‰, -5‰, 0‰, +5‰, +10‰, +15‰, +20‰)  
 5 as a function of precipitation temperature (Friedman and O'Neil, 1977). The contours  
 6 (SMOW) represent oxygen isotopic composition of carbonate balanced fluids. The  
 7  $\delta^{18}\text{O}_{\text{water (SMOW)}}$  values of carbonate balanced fluids within the  $T_3x^2$  sandstones  
 8 originate from the Liu et al., 2014a,b and Shen et al.,2010. The green shapes were  
 9 bounded by the authigenic carbonate cements and the  $\delta^{18}\text{O}_{\text{water (SMOW)}}$  values of  
 10 carbonate balanced fluids.



1

2

Fig. 21. Scatter diagram between the mineral content and major elements abundances in the in the  $T_3x^2$  sandstones. The mineral content were measured by the XRD (data from the table 1 and Fig.12).The major elements abundances were measured by the XRF (data from table 6 and Fig.12).

6

7

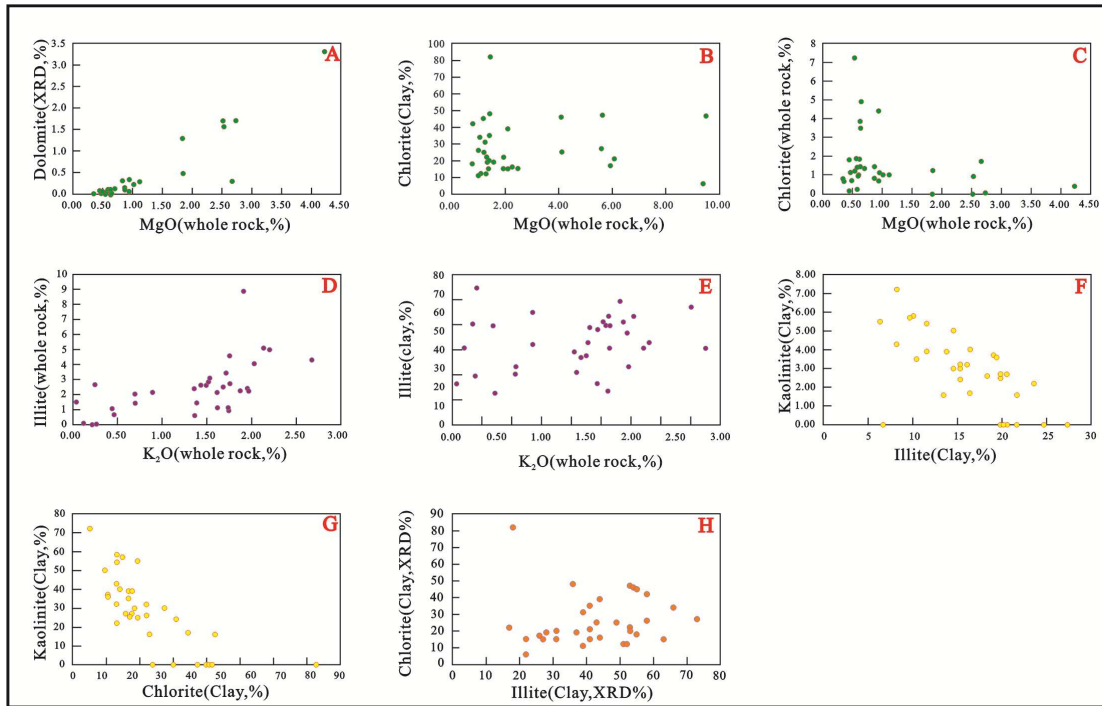
8

9

10

11

12



1

2 Fig. 22. Scatter diagram between the mineral content and major elements abundances  
 3 in the in the  $T_3x^4$  sandstones. The mineral content were measured by the XRD (data  
 4 from the table 2 and Fig.13).The major elements abundances were measured by the  
 5 XRF (data from table 7 and Fig.13).

6

7

8

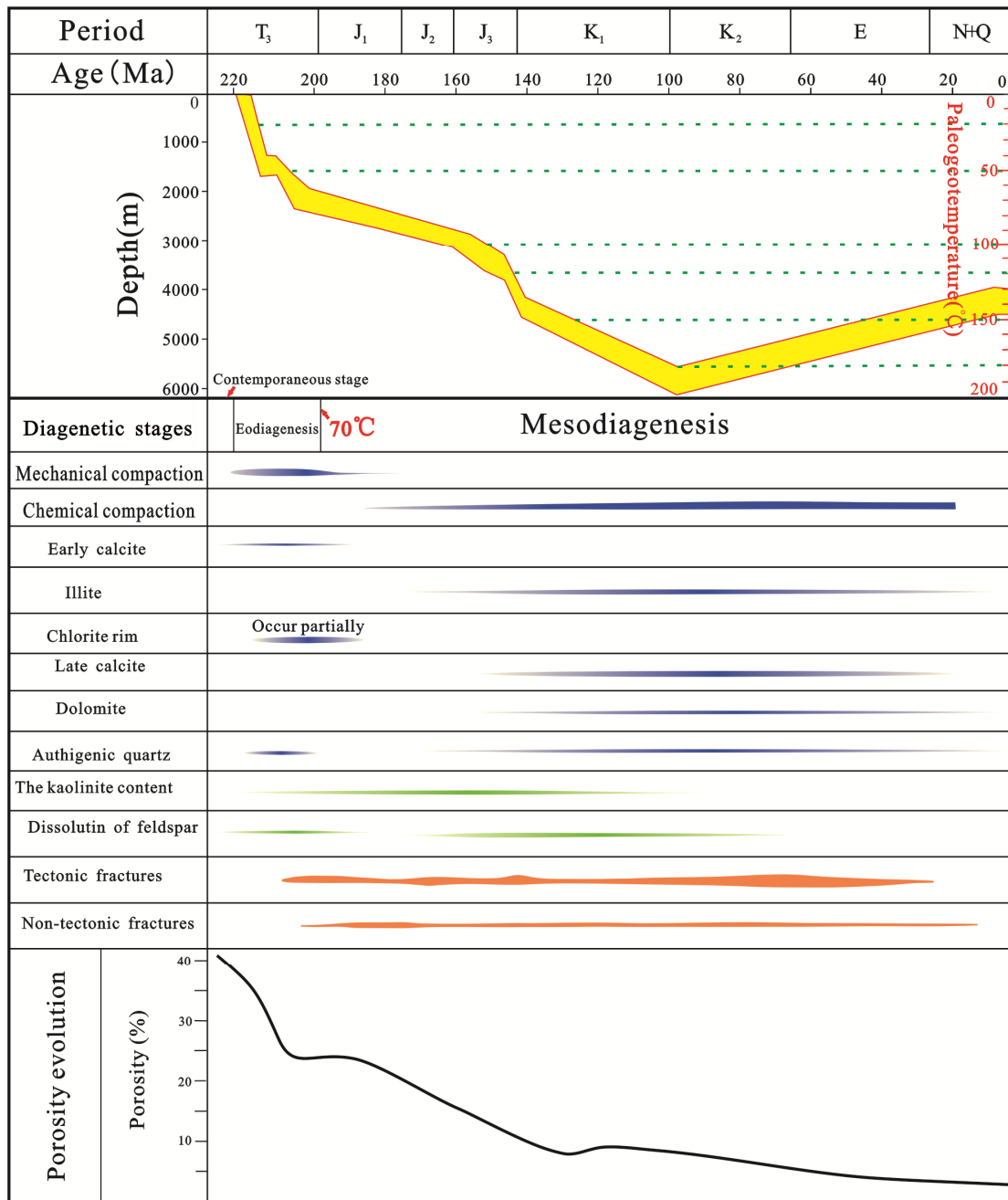
9

10

11

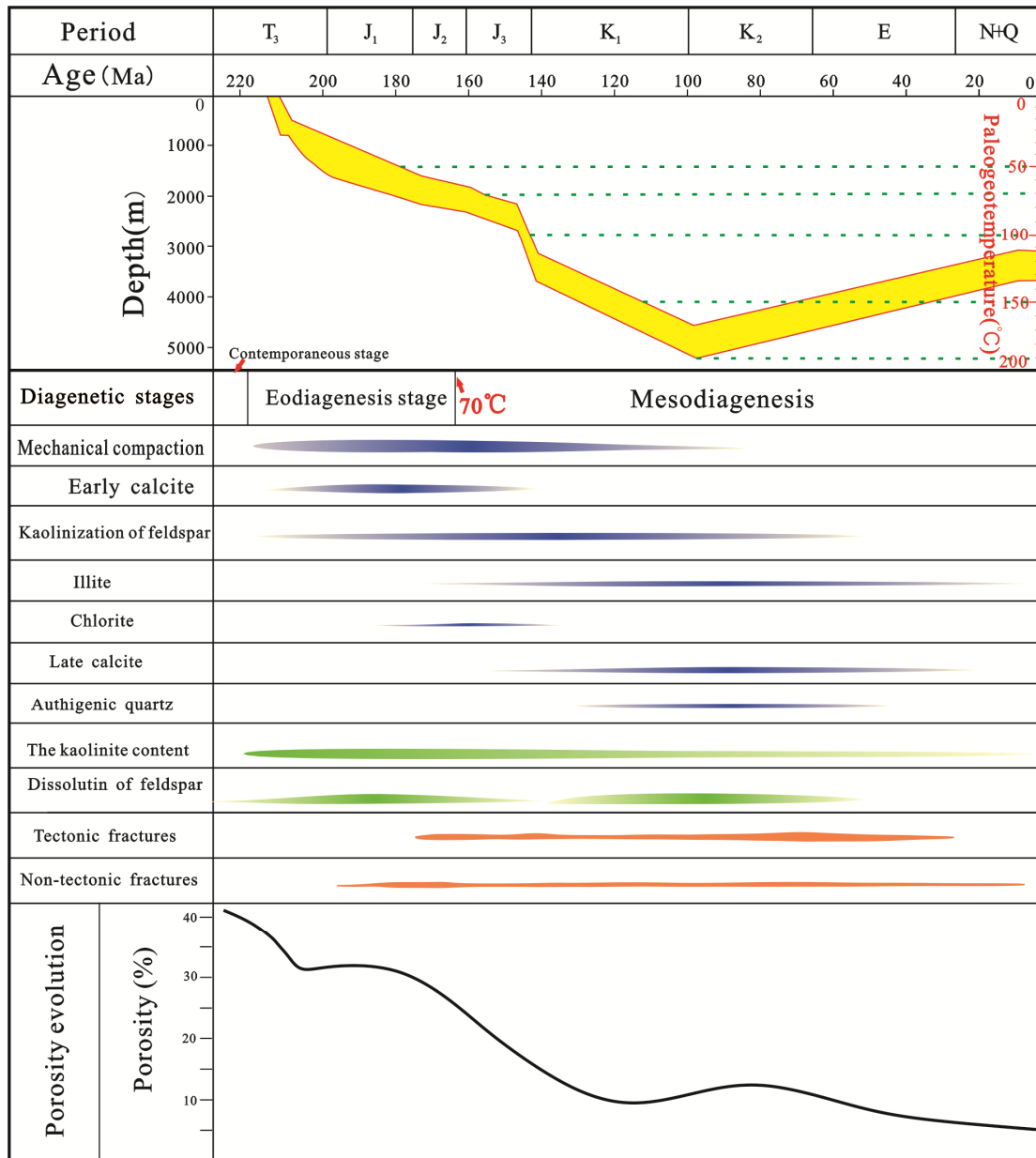
12

13



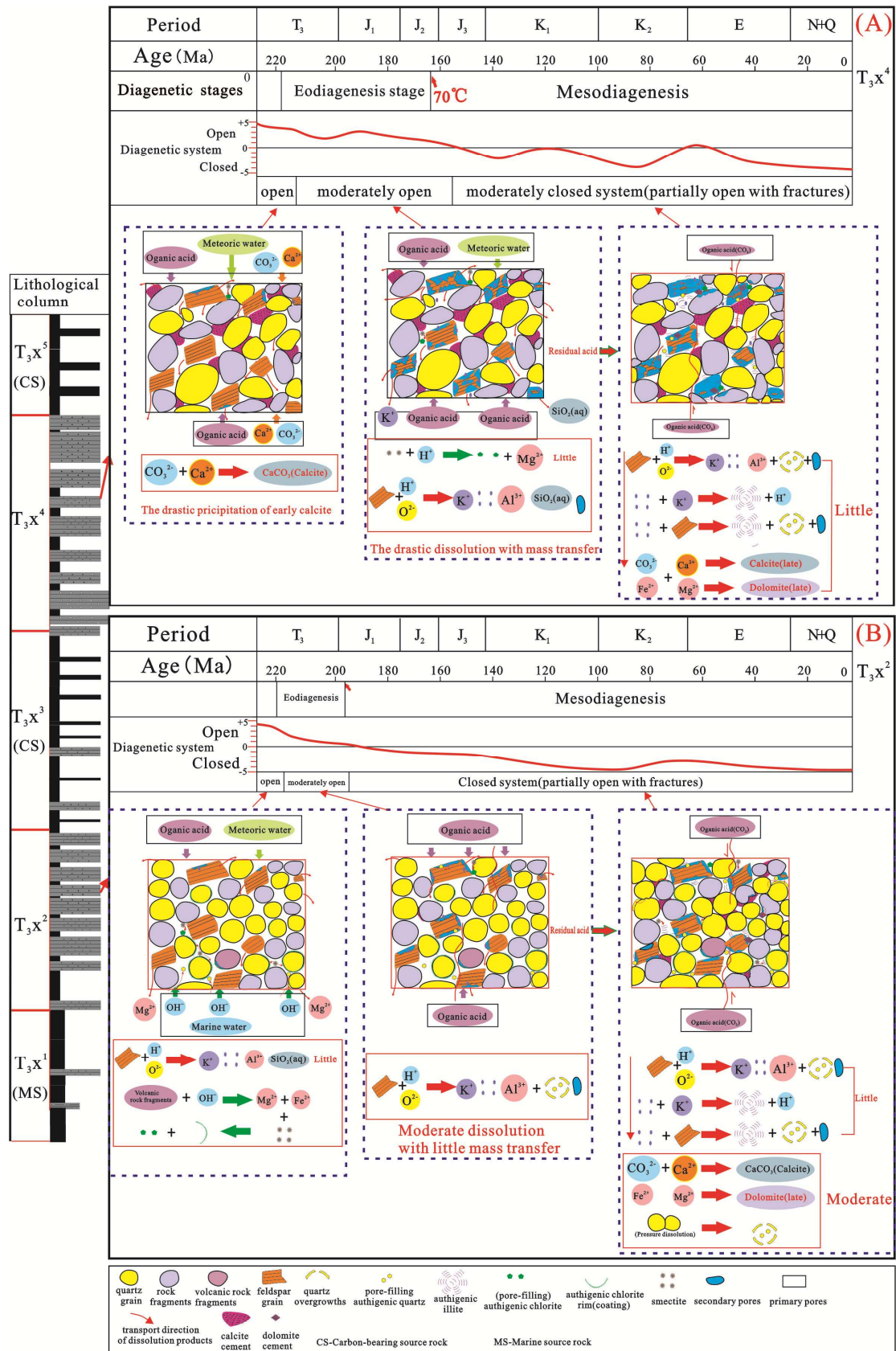
1

2 Fig. 23. Burial, thermal, diagenetic history and evolution of porosity in the T<sub>3</sub>X<sup>2</sup>  
 3 sandstone. The paragenetic sequence showing the relative timing and strength of the  
 4 diagenesis based on petrographic relationships, diagenetic characters and fluid  
 5 inclusion. Burial and thermal history, porosity evolution and the characteristics of  
 6 fractures were presented on the basis of previous studies (Zhang,2005; Zeng,2010;  
 7 Luo ,2015).



1

2 Fig. 24. Burial, thermal, diagenetic history and evolution of porosity in the T<sub>3</sub>X<sup>4</sup>  
3 sandstone. The paragenetic sequence showing the relative timing and strength of the  
4 diagenetic alterations relying on petrographic relationships, diagenetic characters  
5 and fluid inclusion. Burial and thermal history, porosity evolution and the  
6 characteristics of fractures were presented on the basis of previous studies  
7 (Zhang,2005; Zeng,2010; Luo ,2015).



1

2 Fig. 25. A conceptual model summarizing the diagenetic system of the T<sub>3</sub>X<sup>4</sup> sandstone3 (A) and T<sub>3</sub>X<sup>2</sup> sandstone (B). This model indicates the origin, diagenetic relationship,

- 1 controlling factors and evolution of diagenetic system.

ACCEPTED MANUSCRIPT



1. Tight deltaic sandstones have undergone obvious changes of geochemical composition
2. Dissolution was main source of pore space in the T<sub>3x2</sub> and T<sub>3x4</sub> sandstones
3. The diagenetic systems were open at near-surface, eodiagenesis and early mesodiagenesis
4. Diagenetic systems were nearly closed in middle-late mesodiagenesis except for fractures zone.
5. Open system produced secondary pores and provided kaolinite and K<sup>+</sup> for illitization.

ACCEPTED MANUSCRIPT